

Embedded Complexity and Quantum Circuit Volume

Zhenyu Du,¹ Zi-Wen Liu,^{2,*} and Xiongfeng Ma^{1,†}

¹*Center for Quantum Information, Institute for Interdisciplinary Information Sciences, Tsinghua University, Beijing, 100084 China*

²*Yau Mathematical Sciences Center, Tsinghua University, Beijing 100084, China*

Quantum circuit complexity is a pivotal concept in quantum information, quantum many-body physics, and high-energy physics. While extensively studied for closed systems, the characterization and dynamics of circuit complexity are little understood for the situation where the system is embedded within a larger system, which encompasses measurement-assisted state preparation. To address this gap, we introduce the notion of embedded complexity, which accounts for both system extensions and measurements. We study the complexity of projected states in a subsystem after measuring its complement and find that in random circuits, the embedded complexity is lower-bounded by the circuit volume—the total number of gates affecting both the subsystem and its complement. This finding indicates that the total cost of preparing the projected state cannot be reduced by leveraging ancillary qubits and measurements in general. Our result underscores the operational meaning of circuit volume, as it characterizes the embedded complexity of the generated state. Specifically, for random circuits or Clifford circuits, we demonstrate a spacetime conversion that concentrates circuit volume onto a subsystem via a random gate teleportation approach. In scenarios of deep thermalization where the system interacts extensively with a larger system, our analysis suggests that the resulting projected states exhibit high complexity. Additionally, we introduce a shadow tomography protocol that employs only ancillary random states and Bell state measurements, circumventing the need to evolve the input state and thereby simplifying experimental controls.

I. INTRODUCTION

The notion of quantum circuit complexity, defined as the minimal number of local gates required to prepare a specific state, holds pivotal importance across various domains ranging from quantum information [1–3] to physics [4–10]. In sharp contrast to usual properties such as entanglement [11] which is bounded by system size, the circuit complexity of a state produced by a quantum circuit can grow with the circuit depth to reach values exponential in system size, providing novel lens on the prolonged evolution of states in a closed system. Beyond closed systems, understanding the properties of a subsystem embedded in a larger system is an important problem in many-body physics, crucial for enhancing our understanding of phenomena like thermalization [12–14] and quantum chaos [15–17]. In entangled many-body quantum systems, a subsystem may exhibit significant entanglement with its extensive complement [18, 19]. Such entanglement behavior is closely connected to information scrambling [20, 21] and plays a vital role in quantum error correction [10, 22]. Moreover, after polynomial time evolution, universal and highly random quantum state ensembles within a subsystem can be encoded in a single state of a large system [23, 24], illustrating the complex and rich properties of a subsystem over extended durations.

Recent advancements across various experimental platforms [25–29] have enhanced our ability to probe subsystem properties through measurements. A fundamental phenomenon, known as deep thermalization, explores the properties of projected ensembles within a subsystem, which are obtained through local projective measurements on its complement. It has been shown that both the first and higher moments of these ensembles converge to thermal values in generic quantum systems [16, 17, 23, 24, 30]. Such findings are theoretically significant in quantum thermodynamics [31] and practically crucial for protocols like benchmarking [24] and shadow tomography [32]. Furthermore, it has been shown that measurements can significantly enhance the entanglement of projected states, proving to be powerful in many-body state preparation and offering valuable insights for many-body physics [18, 19, 33–38]. Projected states have also been explored in the context of holography [39]. The insights from these studies emphasize the critical importance of thoroughly understanding the complexity of projected states, particularly in the context of state preparation assisted by ancillary qubits and measurements.

Our study addresses this problem by establishing general bounds on the complexity of projected states. We first formally introduce the concept of embedded complexity, which encapsulates the use of ancillary qubits and measurements. With deep origins in holographic quantum gravity, Brown and Susskind proposed a conjecture that

* zwliu0@tsinghua.edu.cn

† xma@tsinghua.edu.cn

for local random circuits, the circuit complexity grows linearly for an exponentially long time [7, 8], which has been proven to various degrees in a series of recent studies [3, 40–42]. These insights underscore a generic phenomenon of the dynamics of complexity in a closed system. Here, we generalize the linear growth result, showing that the complexity of projected states within a subsystem is generally lower-bounded by the quantum circuit volume—the total number of gates deployed across both the subsystem and the ancillary system. Our results indicate that using ancillary qubits and measurements does not significantly reduce the overall number of gates required to prepare the projected state, thereby uncovering a universal behavior of embedded complexity. This finding has profound implications for the quantum volume metric [43, 44], which is widely used to benchmark the capability of quantum systems. We show that the quantum circuit volume effectively captures the ability to generate states within a subsystem that exhibit comparable state complexity, thus providing a practical operational meaning to this metric.

We further demonstrate a spacetime conversion for random circuits or Clifford circuits via a random gate teleportation protocol. This protocol leverages ancillary qubits and measurements to concentrate circuit volume to a specific subsystem. Consequently, the random circuits on the subsystem are capable of generating a state design whose order scales linearly with the circuit volume [42]. This approach ties circuit volume directly to a quantum device’s capability to apply these circuits within a designated subsystem.

Then, based on the random gate teleportation technique, we propose an ancilla-assisted shadow tomography protocol. This protocol performs Bell state measurements on single copies of the input state and ancillary random states and harnesses the measurement outcomes to predict properties of quantum states. This protocol achieves performance comparable to existing shadow tomography methods [32, 45–48], while significantly simplifying experimental requirements by obviating the need for evolving the input state under random unitaries or Hamiltonian dynamics.

II. CIRCUIT MODEL AND EMBEDDED COMPLEXITY

We employ the following local random circuit model to examine the typical behaviors of quantum circuits. The model is extendable to higher dimensions and various architectures. As depicted in Fig. 1(b), an m -qubit local random circuit U with depth d is constructed as $U = U^{(d)}U^{(d-1)}\dots U^{(1)}$, where $U^{(1)} = U_{1,2}^{(1)} \otimes U_{3,4}^{(1)} \otimes \dots$ and subsequent layers $U^{(2)}, U^{(3)}, \dots, U^{(d)}$ follow $U^{(1)}$ in a staggered arrangement. Each two-qubit gate $U_{j,j+1}^{(i)}$ in the i -th layer acts on qubits j and $j+1$, selected randomly according to the Haar measure on $SU(4)$. The ensemble of local random circuits on m qubits with depth d is denoted by $\mathcal{U}_{m,d}$. The ensemble of quantum states created by applying a unitary $U \in \mathcal{U}_{m,d}$ to the initial state $|0\rangle^{\otimes m}$ is represented by:

$$\mathcal{S}_{m,d} = \{U |0\rangle^{\otimes m} : U \in \mathcal{U}_{m,d}\}. \quad (1)$$

The circuits in $\mathcal{U}_{m,d}$ and the states in $\mathcal{S}_{m,d}$ follow probability distributions determined by the Haar measure of each two-qubit gate.

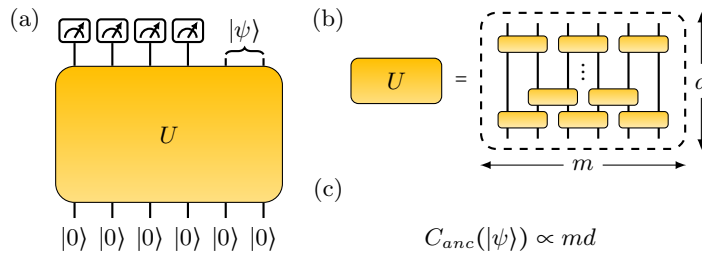


FIG. 1. Embedded complexity and quantum circuit volume. (a) In this work, we consider the embedded complexity of projected states in a small subsystem obtained by applying a quantum circuit U to the initial zero state and performing local projective measurements on its complement. (b) The unitary U is randomly drawn from the m -qubit local random unitaries ensemble $\mathcal{U}_{m,d}$, generated by random circuits composed of staggered two-qubit gates with circuit depth d . (c) Theorem 1 shows that with unit probability, the embedded complexity $C_{anc}(|\psi\rangle)$ of the projected state $|\psi\rangle$ in the small subsystem is lower-bounded by the circuit volume.

We study the complexity of projected state $|\psi\rangle$ in an n -qubit subsystem. As shown in Fig. 1(a), the projected state $|\psi\rangle$ is obtained by first evolving a local random circuit $U \in \mathcal{U}_{m,d}$ on the initial state $|0\rangle^{\otimes m}$ in a larger m -qubit system, followed by measurements on its complement. If the measurement outcome is $a \in \{0, 1\}^{m-n}$, then the projected state can be written as:

$$|\psi\rangle \propto (\langle a| \otimes \mathbb{I}_n) U |0\rangle^{\otimes m} \quad (2)$$

up to a normalization factor. The circuit volume, V , represents the total number of two-qubit gates that generate a state. As shown in Fig. 1(b), the circuit volume used to generate the projected state scales with the product of the number of qubits m and the circuit depth d :

$$V = \lfloor m/2 \rfloor d. \quad (3)$$

Quantum circuit complexity is defined as the minimal circuit volume required to generate the state across all possible circuits [49]. The gates in the circuit are arbitrary unitaries from $SU(4)$ and may act on any pair of sites with no constraints regarding geometric locality. As mentioned, utilizing ancillary qubits and mid-circuit measurement has been recently extensively studied as a powerful approach for quantum state preparation [18, 19, 34–38]. We define embedded complexity to incorporate these operations.

Definition 1 (Embedded complexity). *The embedded complexity $C_{anc}(|\psi\rangle)$ of a pure n -qubit state $|\psi\rangle$ is defined as the minimal number of two-qubit gates required to generate $|\psi\rangle$ within an n -qubit subsystem embedded in a m -qubit larger system. Single-qubit computational-basis measurements and post-selection are allowed in the middle of the circuit:*

$$C_{anc}(|\psi\rangle) := \min\{V : \exists m \geq n, c > 0, |\psi\rangle \otimes |0\rangle^{\otimes(m-n)} = c \Pi_V U_V \Pi_{V-1} U_{V-1} \cdots \Pi_1 U_1 |0\rangle^{\otimes m}\} \quad (4)$$

The two-qubit gates U_i can be arbitrary unitaries in $SU(4)$ and may act on any pair of qubits. The projective operator Π_i acts on the same pair of qubits as U_i ,

$$\begin{aligned} \Pi_i &= P_{i,1} \otimes P_{i,2}, \\ P_{i,1}, P_{i,2} &\in \{\mathbb{I}, |0\rangle\langle 0|, |1\rangle\langle 1|\}. \end{aligned} \quad (5)$$

In defining the embedded complexity, the projected operator Π_i facilitates mid-circuit measurement and post-selection, while the real number c serves as the normalization factor.

III. BOUNDING EMBEDDED COMPLEXITY BY CIRCUIT VOLUME

To determine the complexity of the projected state $|\psi\rangle$, one must take minimization over all possible circuits and measurements that can generate the state. This task is generally challenging due to the difficulty in conclusively eliminating the possibility of reducing the number of gates. Particularly when the subsystem is substantially smaller than the total system size, i.e., $n \ll m$, the possibility becomes more plausible since most two-qubit gates fall outside the light cone of the subsystem. Remarkably, we show that when the measurement result from the complement system is obtained, the complexity of the projected state in the subsystem is lower-bounded by the circuit volume V , as illustrated in Fig. 1(c).

Theorem 1. *Given $m \geq n \geq 4$, consider a local random circuit $U \in \mathcal{U}_{m,d}$ acting on the initial state $|0\rangle^{\otimes m}$. After the first $m-n$ qubits of the state $U|0\rangle^{\otimes m}$ are measured in the computational basis, the projected state $|\psi\rangle$ on the remaining n qubits will, with unit probability, satisfy:*

$$C_{anc}(|\psi\rangle) \geq \min\left(\frac{md}{2n^2} - 2m, 2^{n+1} - 2\right) / 15. \quad (6)$$

For $d = \Omega(n^2)$, the bound can be made $\Omega(\min(\frac{V}{n^2}, 2^n))$, where $V = \lfloor m/2 \rfloor d$ is the circuit volume.

The complete proof of Theorem 1 can be found in Appendix B. Our result shows that the minimal circuit volume required to generate the projected state is lower-bounded by the original circuit volume V , scaled by a factor of $O(\frac{1}{n^2})$, where n represents the size of the subsystem. This finding suggests that, in almost all cases, the utilization of ancillary qubits and measurements does not permit a substantial reduction of the circuit volume V , particularly when the size n of the subsystem is considerably smaller than the size m of the larger system. Consequently, more time is generally required to prepare the projected state in a closed system. This result reveals a fundamental relation between space and time complexity, highlighting how the spatial dimensions of a system directly influence the complexity of the states it can generate in a subsystem. This relation gives the operational meaning of circuit volume as generating states on a subsystem that has comparable complexity. It also offers a fresh perspective on the deep thermalization phenomenon by showing that the projected states are not only highly random [16, 17, 23, 30, 31] but also exhibit high complexity.

IV. SPACETIME CONVERSION FOR RANDOM CIRCUITS AND CLIFFORD CIRCUITS

We also present an explicit construction to show a spacetime conversion for random circuits. The main tool is teleporting random gates between subsystems by Bell state measurement, which we call random gate teleportation. Informally, one prepares the Choi states of random circuits in different subsystems, then performs Bell state measurements to concentrate all the random gates in a small subsystem. The gate teleportation may introduce Pauli errors interleaved in the circuits. Thanks to the property of the Haar measure, these Pauli errors can be absorbed into the random gates. Finally, we obtain a random circuit in a subsystem with increased circuit depth. The protocol is summarized below and illustrated in Fig. 2. See Appendix A for the detailed proof.

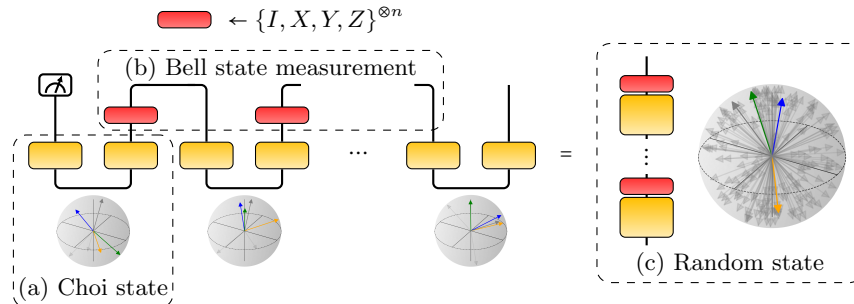


FIG. 2. Spacetime conversion for random circuits via random gate teleportation. (a) This protocol first prepares Choi states of random circuits in different subsystems with circuit depth d . (b) Bell state measurements are then performed to teleport random circuits (yellow rectangle) from one subsystem to another, which may introduce Pauli errors P (red rectangle). P is uniformly distributed on $\{I, X, Y, Z\}^{\otimes n}$. Thanks to the properties of random circuits, these Pauli errors can be absorbed into the random gates. (c) Finally, a random state in $\mathcal{S}_{n,t}$ is prepared with reduced circuit depth d .

Theorem 2. *Given a circuit depth t , for an integer $k \geq 2$, quantum circuits on kn qubits with a reduced depth $d = \lfloor \frac{t}{k} \rfloor + 4$ is sufficient to:*

1. Generate a random state in $\mathcal{S}_{n,t}$.
2. Apply a random gate U from $\mathcal{U}_{n,t}$ to any input state $|\phi\rangle$ when k is an odd number.

Notably, previous work has focused on the projected states sampled from a single state, where the randomness in the state ensemble is originated from measurements [23]. Here, our approach integrates randomness from both measurements and quantum gates that generate the state. By incorporating additional randomness from quantum gates, we can sample random circuits with a comparable volume within a small subsystem, forming an approximate state design whose order scales linearly with circuit volume [42]. Furthermore, these projected states have an approximate complexity that is lower-bounded by circuit volume [3]. See Appendix C for more detailed discussions.

Our approach is closely connected to measurement-based methods for preparing random states [50–52]. Both methods utilize additional qubits and measurements to perform gates on a specific subsystem. The measurement-based protocol can generate random states via constant-depth circuits [52]. At the same time, our result extends beyond constant depth by demonstrating that additional qubits can be used to reduce circuit depth in the intermediate regime, interpolating between the closed system circuit and measurement-based method. A similar spacetime conversion for implementing Clifford circuits is also established in Appendix A. Our results give an operational meaning of circuit volume by showing its utility in quantifying the volume of random and Clifford circuits that can be applied to a subsystem, providing a new perspective on the quantum volume metric [43, 44]. This concept is illustrated in Fig. 3.

V. ANCILLA-ASSISTED SHADOW TOMOGRAPHY

We have shown that performing Bell state measurements can teleport random gates between subsystems. Building on this, we introduce an ancilla-assisted variant of the shadow tomography protocol, which aims to measure the properties of a state of interest ρ , accessible at the beginning of each experiment.

Our protocol is inspired by the classical shadow protocol [45] that has drawn substantial recent interest. In the original classical shadow protocol, the states are measured in randomized bases, and this randomness is introduced by applying random unitaries U to the input state $\rho \mapsto U\rho U^\dagger$. To estimate many important properties of the input state

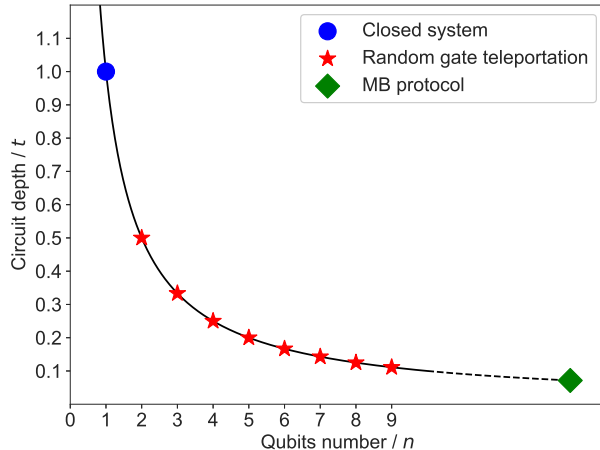


FIG. 3. The quantum resources required to generate the random state ensemble $\mathcal{S}_{n,t}$. Random gate teleportation protocols allow for reduced circuit depth using additional qubits and Bell state measurements, while maintaining the same circuit volume as direct implementations in closed systems. This method interpolates between closed-system circuits and measurement-based (MB) protocols, which can generate $\mathcal{S}_{n,t}$ within a constant depth [50–52]. This figure also illustrates the quantum resources required to implement Clifford circuits.

ρ , such as overlap fidelities with respect to many target states, one needs to apply global random unitaries. This poses a major challenge for current quantum devices due to the highly sophisticated experimental controls required. Recent research has focused on easing the experimental requirement for classical shadow, such as developing shallow-depth classical shadow protocols [46, 47], or replacing the random unitaries with Hamiltonian evolutions [32, 48, 53].

Here, we propose a protocol that avoids evolving the state ρ under random unitaries or Hamiltonian dynamics. The key idea is to introduce the randomness from the ancillary system and Bell state measurements. We present the ancilla-assisted shadow tomography protocol in Box 1 and depict it in Fig. 4.

Box 1: Ancilla-assisted shadow tomography

Input:

N copies of an n -qubit state ρ .

Protocol:

1. Select an n -qubit state ensemble \mathcal{S} .
2. For each copy of input state ρ , randomly draw a state $|\phi\rangle \in \mathcal{S}$.
3. Perform Bell state measurement between $|\phi\rangle$ and ρ , and record the measurement result.
4. Obtain N data points by repeating Steps 2 to Step 3 on N copies of ρ .
5. Process the measurement results on classical computers to predict properties of the state ρ .

Although reconstructing the state requires exponentially many experiments, our primary motivation is to measure properties instead of fully recovering the state ρ . In Appendix D, we provide further analysis of our protocol. We use measurement results to construct unbiased estimators $\hat{\sigma}$ of ρ , allowing us to obtain an unbiased estimator $\text{tr}(O\hat{\sigma})$ of the expectation value $\text{tr}(O\rho)$. We show that when the state ensemble is selected as a state 3-design or as local random states, our protocol achieves performance comparable to that of the classical shadow protocol.

Theorem 3. *To predict the expectation value of M observables $\text{tr}(O_1\rho), \text{tr}(O_2\rho), \dots, \text{tr}(O_M\rho)$ to additive error ϵ , the ancilla-assisted shadow tomography protocol requires N copies of input state ρ , where:*

1. $N = O\left(\frac{\log M}{\epsilon^2} \max_i \text{tr}(O_i^2)\right)$ when \mathcal{S} is chosen as a state 3-design.

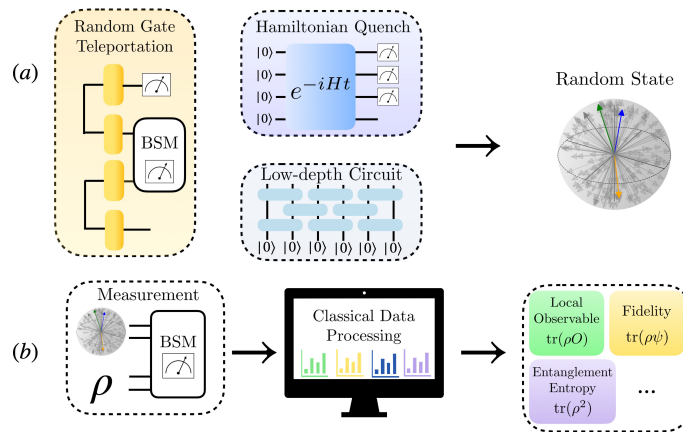


FIG. 4. The ancilla-assisted shadow tomography protocol. (a) This protocol requires ancillary random states $|\phi\rangle$. The choice of the random state offers a large degree of freedom, providing the protocol with significant generality. For example, the states can be prepared through random gate teleportation proposed in this work, requiring smaller circuit depth, or via the projected ensemble of Hamiltonian quenches [23], potentially applicable in analog quantum simulators. The shallow classical shadow [46, 47] can also be adopted into this protocol by preparing the random states via low-depth random circuits. (b) The protocol acquires classical data by performing Bell state measurements (BSM) on the input state ρ and ancillary random states. The measurement data can later be utilized to predict many properties of ρ through classical data processing, such as the expectation values of observables, state fidelity, and nonlinear functions like the second-order Rényi entropy.

2. $N = O(\frac{\log M}{\epsilon^2} \max_i 4^{k_i})$ when \mathcal{S} is chosen as ensemble of local random states $|\phi\rangle = |\phi_1\rangle \otimes |\phi_2\rangle \otimes \dots \otimes |\phi_n\rangle$, where each $|\phi_i\rangle$ is uniformly drawn from

$$\{|0\rangle, |+\rangle = \frac{1}{\sqrt{2}}(|0\rangle + |1\rangle), |+i\rangle = \frac{1}{\sqrt{2}}(|0\rangle + i|1\rangle)\}.$$

Here, k_i is the locality of observable O_i , and $\max_i \|O_i\|_\infty \leq 1$.

Moreover, we can predict nonlinear functions $f(\rho)$, such as the second-order Rényi entropy $\text{tr}(\rho^2)$, by utilizing the U statistics to construct unbiased estimators of $\rho^{\otimes k}$ via N independent unbiased estimator $\{\hat{\sigma}_i\}$ of ρ [32, 45, 54]:

$$\binom{N}{k}^{-1} \sum_{1 \leq i_1, \dots, i_k \leq N} \hat{\sigma}_{i_1} \otimes \hat{\sigma}_{i_2} \otimes \dots \otimes \hat{\sigma}_{i_k}. \quad (7)$$

A key benefit of our protocol is that it eliminates the need to evolve the input states, which is particularly suitable for practical scenarios where preparing ancillary states is more accessible than evolving the input state, thus may significantly ease experimental implementation. Additionally, our protocol exhibits substantial flexibility in selecting ancillary state ensembles, which can be easily adapted to different variations of shadow tomography, such as shallow classical shadows [46, 47], Hamiltonian-driven classical shadow [32, 48] and thrifty shadow estimation protocol [55, 56].

The flexibility in preparing ancillary states further simplifies experimental setups. For instance, when choosing \mathcal{S} as a global random state ensemble, the state $|\phi\rangle \in \mathcal{S}$ can be prepared through random or Clifford circuits via the random gate teleportation protocol, which can reduce the circuit depth. Additionally, recent studies have demonstrated that random states can be prepared by measuring subsystems of a state evolved under Hamiltonian quenches [23, 24]. This state preparation method can be utilized in our protocol to simplify experimental control further and can be implemented in current analog quantum simulators.

VI. DISCUSSION

We show that embedded complexity is generally lower-bounded by circuit volume in local random circuits. Additionally, we observe that approximate complexity can also be lower-bounded by circuit volume in the random gate teleportation protocols, implying that this lower bound may be generic in random circuits. The rigorous extension of our results to approximate version provides an opportunity for future work.

We illustrate a spacetime conversion for sampling random states in a subsystem, where these states constitute an approximate state design that scales linearly with circuit volume. This connection between state design and circuit

volume suggests the possibility of sampling higher-order state designs in a subsystem through partially measuring states within a state design of a larger system. Future research on this conversion remains a valuable avenue for exploring the deep thermalization phenomenon and developing efficient methods for sampling random states [57–62], which has wide-ranging applications in quantum information from learning [32, 45, 53] to benchmarking [24, 63–65].

Expanding the operational meaning of quantum circuit volume beyond the realms of random and Clifford circuits is essential for assessing the computational capabilities of quantum devices. This exploration includes the intriguing possibility of employing Clifford circuits interspersed with T gates [66, 67]. It is also worthwhile to explore connections of our results to the burgeoning field of many-body state preparation with measurements [18, 19, 34–38], and furthermore, related physical contexts, particularly phases of matter, gauge theory, and holographic complexity. Finally, we also anticipate further theoretical and experimental exploration of the ancilla-assisted shadow tomography protocol and investigations on applying random gate teleportation in other randomized schemes, such as randomized benchmarking [63, 64] and randomized compiling [68, 69].

ACKNOWLEDGMENTS

The authors thank Junjie Chen, Zhenhuan Liu, Yuxuan Yan, Xiao Yuan, and Qi Zhao for their helpful discussion. This work is supported by the National Natural Science Foundation of China Grants No. 12174216 and the Innovation Program for Quantum Science and Technology Grant No. 2021ZD0300804 and No. 2021ZD0300702. Z.-W.L. is supported in part by a startup funding from YMSC, Tsinghua University.

-
- [1] S. Aaronson, “The complexity of quantum states and transformations: From quantum money to black holes,” (2016), [arXiv:1607.05256](#).
- [2] A. Bouland, B. Fefferman, and U. Vazirani, in *11th Innovations in Theoretical Computer Science Conference (ITCS 2020)*, Leibniz International Proceedings in Informatics (LIPIcs), Vol. 151, edited by T. Vidick (Schloss Dagstuhl – Leibniz-Zentrum für Informatik, Dagstuhl, Germany, 2020) pp. 63:1–63:2.
- [3] F. G. Brandão, W. Chemissany, N. Hunter-Jones, R. Kueng, and J. Preskill, *PRX Quantum* **2** (2021), [10.1103/prxquantum.2.030316](#).
- [4] D. Stanford and L. Susskind, *Physical Review D* **90** (2014), [10.1103/physrevd.90.126007](#).
- [5] L. Susskind, *Fortschritte der Physik* **64**, 24–43 (2016).
- [6] A. R. Brown, D. A. Roberts, L. Susskind, B. Swingle, and Y. Zhao, *Physical Review D* **93** (2016), [10.1103/physrevd.93.086006](#).
- [7] A. R. Brown and L. Susskind, *Physical Review D* **97** (2018), [10.1103/physrevd.97.086015](#).
- [8] L. Susskind, “Black holes and complexity classes,” (2018), [arXiv:1802.02175 \[hep-th\]](#).
- [9] X.-G. Wen, *ISRN Condensed Matter Physics* **2013**, 198710 (2013).
- [10] J. Yi, W. Ye, D. Gottesman, and Z.-W. Liu, “Complexity and order in approximate quantum error-correcting codes,” (2024), [arXiv:2310.04710 \[quant-ph\]](#).
- [11] A. Nahum, J. Ruhman, S. Vijay, and J. Haah, *Physical Review X* **7** (2017), [10.1103/physrevx.7.031016](#).
- [12] M. Rigol, V. Dunjko, and M. Olshanii, *Nature* **452**, 854–858 (2008).
- [13] A. M. Kaufman, M. E. Tai, A. Lukin, M. Rispoli, R. Schittko, P. M. Preiss, and M. Greiner, *Science* **353**, 794–800 (2016).
- [14] D. A. Abanin, E. Altman, I. Bloch, and M. Serbyn, *Rev. Mod. Phys.* **91**, 021001 (2019).
- [15] L. D’Alessio, Y. Kafri, A. Polkovnikov, and M. Rigol, *Advances in Physics* **65**, 239–362 (2016).
- [16] W. W. Ho and S. Choi, *Physical Review Letters* **128** (2022), [10.1103/physrevlett.128.060601](#).
- [17] M. Ippoliti and W. W. Ho, *PRX Quantum* **4** (2023), [10.1103/prxquantum.4.030322](#).
- [18] T.-C. Lu, L. A. Lessa, I. H. Kim, and T. H. Hsieh, *PRX Quantum* **3** (2022), [10.1103/prxquantum.3.040337](#).
- [19] N. Tantivasadakarn, R. Thorngren, A. Vishwanath, and R. Verresen, *Physical Review X* **14** (2024), [10.1103/physrevx.14.021040](#).
- [20] A. Nahum, S. Vijay, and J. Haah, *Physical Review X* **8** (2018), [10.1103/physrevx.8.021014](#).
- [21] X. Mi, P. Roushan, C. Quintana, S. Mandrà, J. Marshall, C. Neill, F. Arute, K. Arya, J. Atalaya, R. Babbush, J. C. Bardin, R. Barends, J. Basso, A. Bengtsson, S. Boixo, A. Bourassa, M. Broughton, B. B. Buckley, D. A. Buell, B. Burkett, N. Bushnell, Z. Chen, B. Chiaro, R. Collins, W. Courtney, S. Demura, A. R. Derk, A. Dunsworth, D. Eppens, C. Erickson, E. Farhi, A. G. Fowler, B. Foxen, C. Gidney, M. Giustina, J. A. Gross, M. P. Harrigan, S. D. Harrington, J. Hilton, A. Ho, S. Hong, T. Huang, W. J. Huggins, L. B. Ioffe, S. V. Isakov, E. Jeffrey, Z. Jiang, C. Jones, D. Kafri, J. Kelly, S. Kim, A. Kitaev, P. V. Klimov, A. N. Korotkov, F. Kostritsa, D. Landhuis, P. Laptev, E. Lucero, O. Martin, J. R. McClean, T. McCourt, M. McEwen, A. Megrant, K. C. Miao, M. Mohseni, S. Montazeri, W. Mruczkiewicz, J. Mutus, O. Naaman, M. Neeley, M. Newman, M. Y. Niu, T. E. O’Brien, A. Opremcak, E. Ostby, B. Pato, A. Petukhov, N. Redd, N. C. Rubin, D. Sank, K. J. Satzinger, V. Shvarts, D. Strain, M. Szalay, M. D. Trevithick, B. Villalonga, T. White, Z. J. Yao, P. Yeh, A. Zalcman, H. Neven, I. Aleiner, K. Kechedzhi, V. Smelyanskiy, and Y. Chen, *Science* **374**, 1479–1483 (2021).

- [22] S. Choi, Y. Bao, X.-L. Qi, and E. Altman, *Physical Review Letters* **125** (2020), 10.1103/physrevlett.125.030505.
- [23] J. S. Cotler, D. K. Mark, H.-Y. Huang, F. Hernández, J. Choi, A. L. Shaw, M. Endres, and S. Choi, *PRX Quantum* **4** (2023), 10.1103/prxquantum.4.010311.
- [24] J. Choi, A. L. Shaw, I. S. Madjarov, X. Xie, R. Finkelstein, J. P. Covey, J. S. Cotler, D. K. Mark, H.-Y. Huang, A. Kale, H. Pichler, F. G. S. L. Brandão, S. Choi, and M. Endres, *Nature* **613**, 468–473 (2023).
- [25] F. Arute, K. Arya, R. Babbush, D. Bacon, J. C. Bardin, R. Barends, R. Biswas, S. Boixo, F. G. S. L. Brandao, D. A. Buell, B. Burkett, Y. Chen, Z. Chen, B. Chiaro, R. Collins, W. Courtney, A. Dunsworth, E. Farhi, B. Foxen, A. Fowler, C. Gidney, M. Giustina, R. Graff, K. Guerin, S. Habegger, M. P. Harrigan, M. J. Hartmann, A. Ho, M. Hoffmann, T. Huang, T. S. Humble, S. V. Isakov, E. Jeffrey, Z. Jiang, D. Kafri, K. Kechedzhi, J. Kelly, P. V. Klimov, S. Knysh, A. Korotkov, F. Kostritsa, D. Landhuis, M. Lindmark, E. Lucero, D. Lyakh, S. Mandrà, J. R. McClean, M. McEwen, A. Megrant, X. Mi, K. Michielsen, M. Mohseni, J. Mutus, O. Naaman, M. Neeley, C. Neill, M. Y. Niu, E. Ostby, A. Petukhov, J. C. Platt, C. Quintana, E. G. Rieffel, P. Roushan, N. C. Rubin, D. Sank, K. J. Satzinger, V. Smelyanskiy, K. J. Sung, M. D. Trevithick, A. Vainsencher, B. Villalonga, T. White, Z. J. Yao, P. Yeh, A. Zalcman, H. Neven, and J. M. Martinis, *Nature* **574**, 505–510 (2019).
- [26] Z. Ni, S. Li, X. Deng, Y. Cai, L. Zhang, W. Wang, Z.-B. Yang, H. Yu, F. Yan, S. Liu, C.-L. Zou, L. Sun, S.-B. Zheng, Y. Xu, and D. Yu, *Nature* **616**, 56–60 (2023).
- [27] W. Cai, X. Mu, W. Wang, J. Zhou, Y. Ma, X. Pan, Z. Hua, X. Liu, G. Xue, H. Yu, H. Wang, Y. Song, C.-L. Zou, and L. Sun, *Nature Physics* **20**, 1022–1026 (2024).
- [28] S. J. Evered, D. Bluvstein, M. Kalinowski, S. Ebadi, T. Manovitz, H. Zhou, S. H. Li, A. A. Geim, T. T. Wang, N. Maskara, H. Levine, G. Semeghini, M. Greiner, V. Vuletić, and M. D. Lukin, *Nature* **622**, 268–272 (2023).
- [29] M. P. da Silva, C. Ryan-Anderson, J. M. Bello-Rivas, A. Chernoguzov, J. M. Dreiling, C. Foltz, F. Frachon, J. P. Gaebler, T. M. Gatterman, L. Grans-Samuelsson, D. Hayes, N. Hewitt, J. Johansen, D. Lucchetti, M. Mills, S. A. Moses, B. Neyenhuis, A. Paz, J. Pino, P. Siegfried, J. Strabley, A. Sundaram, D. Tom, S. J. Wernli, M. Zanner, R. P. Stutz, and K. M. Svore, “Demonstration of logical qubits and repeated error correction with better-than-physical error rates,” (2024), [arXiv:2404.02280 \[quant-ph\]](https://arxiv.org/abs/2404.02280).
- [30] T. Bhore, J.-Y. Desaulles, and Z. Papić, *Phys. Rev. B* **108**, 104317 (2023).
- [31] D. K. Mark, F. Surace, A. Elben, A. L. Shaw, J. Choi, G. Refael, M. Endres, and S. Choi, “A maximum entropy principle in deep thermalization and in hilbert-space ergodicity,” (2024), [arXiv:2403.11970 \[quant-ph\]](https://arxiv.org/abs/2403.11970).
- [32] M. C. Tran, D. K. Mark, W. W. Ho, and S. Choi, *Physical Review X* **13** (2023), 10.1103/physrevx.13.011049.
- [33] H. J. Briegel and R. Raussendorf, *Phys. Rev. Lett.* **86**, 910 (2001).
- [34] L. Piroli, G. Styliaris, and J. I. Cirac, *Physical Review Letters* **127** (2021), 10.1103/physrevlett.127.220503.
- [35] R. Verresen, N. Tantivasadakarn, and A. Vishwanath, “Efficiently preparing schrödinger’s cat, fractons and non-abelian topological order in quantum devices,” (2022), [arXiv:2112.03061 \[quant-ph\]](https://arxiv.org/abs/2112.03061).
- [36] S. Bravyi, I. Kim, A. Kliesch, and R. Koenig, “Adaptive constant-depth circuits for manipulating non-abelian anyons,” (2022), [arXiv:2205.01933 \[quant-ph\]](https://arxiv.org/abs/2205.01933).
- [37] N. Tantivasadakarn, R. Verresen, and A. Vishwanath, *Physical Review Letters* **131** (2023), 10.1103/physrevlett.131.060405.
- [38] T.-C. Lu, Z. Zhang, S. Vijay, and T. H. Hsieh, *PRX Quantum* **4** (2023), 10.1103/prxquantum.4.030318.
- [39] S.-K. Jian and Y. Zhang, *Journal of High Energy Physics* **2024** (2024), 10.1007/jhep05(2024)241.
- [40] J. Haferkamp, P. Faist, N. B. T. Kothakonda, J. Eisert, and N. Yunger Halpern, *Nature Physics* **18**, 528–532 (2022).
- [41] Z. Li, “Short proofs of linear growth of quantum circuit complexity,” (2022), [arXiv:2205.05668 \[quant-ph\]](https://arxiv.org/abs/2205.05668).
- [42] C.-F. Chen, J. Haah, J. Haferkamp, Y. Liu, T. Metger, and X. Tan, “Incompressibility and spectral gaps of random circuits,” (2024), [arXiv:2406.07478](https://arxiv.org/abs/2406.07478).
- [43] A. W. Cross, L. S. Bishop, S. Sheldon, P. D. Nation, and J. M. Gambetta, *Physical Review A* **100** (2019), 10.1103/physreva.100.032328.
- [44] C. H. Baldwin, K. Mayer, N. C. Brown, C. Ryan-Anderson, and D. Hayes, *Quantum* **6**, 707 (2022).
- [45] H.-Y. Huang, R. Kueng, and J. Preskill, *Nature Physics* **16**, 1050–1057 (2020).
- [46] H.-Y. Hu, S. Choi, and Y.-Z. You, *Phys. Rev. Res.* **5**, 023027 (2023).
- [47] C. Bertoni, J. Haferkamp, M. Hinsche, M. Ioannou, J. Eisert, and H. Pashayan, *Phys. Rev. Lett.* **133**, 020602 (2024).
- [48] Z. Liu, Z. Hao, and H.-Y. Hu, “Predicting arbitrary state properties from single hamiltonian quench dynamics,” (2024), [arXiv:2311.00695 \[quant-ph\]](https://arxiv.org/abs/2311.00695).
- [49] Here, the basic gate components are considered as two-qubit gates. We can also consider k -local gates as basic gates. Since any k -local gate can be decomposed into $\exp(O(k))$ two-qubit gates, this change in basic gates results in at most $\exp(O(k))$ scaling of state complexity, which remains a constant when k is a constant.
- [50] D. Gottesman and I. L. Chuang, *Nature* **402**, 390–393 (1999).
- [51] R. Raussendorf and H. J. Briegel, *Phys. Rev. Lett.* **86**, 5188 (2001).
- [52] P. S. Turner and D. Markham, *Physical Review Letters* **116** (2016), 10.1103/physrevlett.116.200501.
- [53] M. McGinley and M. Fava, *Physical Review Letters* **131** (2023), 10.1103/physrevlett.131.160601.
- [54] W. Hoeffding, *The Annals of Mathematical Statistics* **19**, 293 (1948).
- [55] J. Helsen and M. Walter, *Physical Review Letters* **131** (2023), 10.1103/physrevlett.131.240602.
- [56] Y. Zhou and Q. Liu, *Quantum* **7**, 1044 (2023).
- [57] A. Ambainis and J. Emerson, in *Twenty-Second Annual IEEE Conference on Computational Complexity (CCC’07)* (IEEE, 2007).
- [58] Y. Nakata, C. Hirche, M. Koashi, and A. Winter, *Physical Review X* **7** (2017), 10.1103/physrevx.7.021006.
- [59] H. Zhu, *Physical Review A* **96** (2017), 10.1103/physreva.96.062336.

- [60] C.-F. Chen, J. Docter, M. Xu, A. Bouland, and P. Hayden, “Efficient unitary t-designs from random sums,” (2024), [arXiv:2402.09335 \[quant-ph\]](#).
- [61] T. Metger, A. Poremba, M. Sinha, and H. Yuen, “Simple constructions of linear-depth t-designs and pseudorandom unitaries,” (2024), [arXiv:2404.12647 \[quant-ph\]](#).
- [62] C.-F. Chen, A. Bouland, F. G. S. L. Brandão, J. Docter, P. Hayden, and M. Xu, “Efficient unitary designs and pseudorandom unitaries from permutations,” (2024), [arXiv:2404.16751 \[quant-ph\]](#).
- [63] E. Knill, D. Leibfried, R. Reichle, J. Britton, R. B. Blakestad, J. D. Jost, C. Langer, R. Ozeri, S. Seidelin, and D. J. Wineland, *Physical Review A* **77** (2008), [10.1103/physreva.77.012307](#).
- [64] R. N. Alexander, P. S. Turner, and S. D. Bartlett, *Physical Review A* **94** (2016), [10.1103/physreva.94.032303](#).
- [65] D. K. Mark, J. Choi, A. L. Shaw, M. Endres, and S. Choi, *Physical Review Letters* **131** (2023), [10.1103/physrevlett.131.110601](#).
- [66] S. Bravyi and D. Gosset, *Physical Review Letters* **116** (2016), [10.1103/physrevlett.116.250501](#).
- [67] C.-Y. Lai and H.-C. Cheng, *IEEE Transactions on Information Theory* **68**, 3951–3964 (2022).
- [68] J. J. Wallman and J. Emerson, *Physical Review A* **94** (2016), [10.1103/physreva.94.052325](#).
- [69] A. Hashim, R. K. Naik, A. Morvan, J.-L. Ville, B. Mitchell, J. M. Kreikebaum, M. Davis, E. Smith, C. Iancu, K. P. O’Brien, I. Hincks, J. J. Wallman, J. Emerson, and I. Siddiqi, *Physical Review X* **11** (2021), [10.1103/physrevx.11.041039](#).
- [70] D. Gottesman, “The heisenberg representation of quantum computers,” (1998), [arXiv:quant-ph/9807006 \[quant-ph\]](#).
- [71] R. Suzuki, J. Haferkamp, J. Eisert, and P. Faist, “Quantum complexity phase transitions in monitored random circuits,” (2023), [arXiv:2305.15475 \[quant-ph\]](#).
- [72] J. Haferkamp, *Quantum* **6**, 795 (2022).
- [73] F. G. S. L. Brandão, A. W. Harrow, and M. Horodecki, *Communications in Mathematical Physics* **346**, 397–434 (2016).

Appendix A: Spacetime conversion for random circuits and Clifford circuits

In this section, we provide the details of the spacetime conversion for random circuits and Clifford circuits. We begin by revisiting a gate teleportation protocol. Then, we prove Theorem 2 in the main text, which shows the spacetime conversion for random circuits. Finally, we extend the spacetime conversion result to Clifford circuits.

1. Preliminaries on gate teleportation

a. Bell state measurement

Firstly, we revisit the notion of Bell state measurement, an important component in gate teleportation. Denote the unnormalized maximally entangled state as:

$$|\Phi\rangle = |00\rangle + |11\rangle. \quad (\text{A1})$$

We can represent $|\Phi\rangle$ using a tensor network diagram, as illustrated in Fig. 5(a).

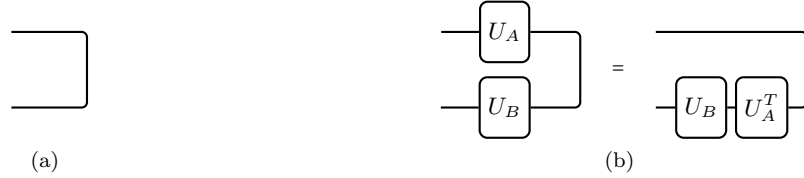


FIG. 5. (a) Tensor network diagram of the unnormalized maximally entangled state $|\Phi\rangle = |00\rangle + |11\rangle$. (b) Diagram illustrating the movement of the unitary on the maximally entangled state. U_A is applied on one side of the unnormalized maximally entangled state and can be moved to the other.

The four Bell states are abbreviated as:

$$|\phi_{ab}\rangle = \frac{1}{\sqrt{2}}(X^a Z^b \otimes \mathbb{I}) |\Phi\rangle, \quad a, b \in \{0, 1\}. \quad (\text{A2})$$

where $|\phi_{00}\rangle$ corresponds to the EPR pairs. We represent $|\phi^n\rangle_{AB}$ as the n EPR pairs on systems A and B :

$$|\phi^n\rangle_{AB} = \bigotimes_{i=1}^n |\phi_{00}\rangle_{A_i, B_i}, \quad (\text{A3})$$

where $A = A_1 A_2 \dots A_n$ and $B = B_1 B_2 \dots B_n$ are n -qubit system. For any n -qubit unitary U , we define the state $|U, V\rangle_{AB}$ as applying U to $|\phi^n\rangle_{AB}$ on subsystem A and V on subsystem B :

$$|U, V\rangle_{AB} = (U \otimes V) |\phi^n\rangle_{AB}. \quad (\text{A4})$$

A beneficial property is that one can move a unitary operation from one side of the maximally entangled state to the other:

$$|U_A, U_B\rangle_{AB} = |\mathbb{I}, U_B U_A^T\rangle_{AB} \quad (\text{A5})$$

where U_A, U_B represents an n -qubit unitaries. The diagram representing Eq. (A5) is shown in Fig. 5(b).

We frequently utilize Bell state measurements in our analysis. Consider a $4n$ -qubit quantum state $|\psi_{ABCD}\rangle$. Suppose Bell state measurements are performed on each A_i and C_i for $1 \leq i \leq n$ in the basis $\{|\phi_{ab}\rangle\}$, and the measurement outcome on the i -th pair of qubits is represented by a_i and b_i , corresponding to the Bell state $|X^{a_i} Z^{b_i}, \mathbb{I}\rangle$. Now, let $\mathbf{a} = a_1 a_2 \dots a_n$ and $\mathbf{b} = b_1 b_2 \dots b_n$. Define $X^{\mathbf{a}} = X^{a_1} \otimes X^{a_2} \otimes \dots \otimes X^{a_n}$ and $Z^{\mathbf{b}}$ analogously. The unnormalized post-measurement state on the system BD after obtaining the measurement result \mathbf{a}, \mathbf{b} is then given by:

$$(|X^{\mathbf{a}} Z^{\mathbf{b}}, \mathbb{I}\rangle_{AC})^\dagger \otimes \mathbb{I}_B \otimes \mathbb{I}_D |\psi_{ABCD}\rangle = (\langle X^{\mathbf{a}} Z^{\mathbf{b}}, \mathbb{I}\rangle_{AC} \otimes \mathbb{I}_B \otimes \mathbb{I}_D) |\psi_{ABCD}\rangle \quad (\text{A6})$$

b. Gate teleportation

In a seminal work on measurement-based quantum computing [50], a construction for gate teleportation is proposed to apply a unitary U to a state $|\psi\rangle$. The essence of this method is to perform Bell state measurements between a state $|\psi\rangle$ and the Choi state of a unitary U instead of directly applying U to $|\psi\rangle$. According to Eq. (A6), a Pauli error is applied before the unitary. This process is illustrated in Fig. 6 and summarized in the following lemma.

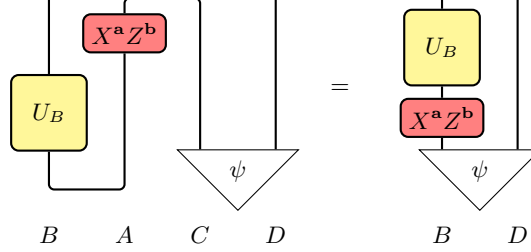


FIG. 6. Gate teleportation with Pauli error. Given two input state $|\mathbb{I}, U_B\rangle_{AB}$ and $|\psi\rangle_{CD}$, the unitary applied on system B can be teleported onto $|\psi\rangle$ via Bell state measurements, up to a Pauli error $P = X^a Z^b$, where \mathbf{a}, \mathbf{b} are the results of the Bell state measurement.

Lemma 1 (Gate teleportation with Pauli error). *Let $|\mathbb{I}, U_B\rangle_{AB}$ and $|\psi\rangle_{CD}$ be two states, where A, B, C, D are n -qubit systems. After performing Bell state measurements on subsystem AC and obtaining measurement results \mathbf{a} and \mathbf{b} , where $\mathbf{a}, \mathbf{b} \in \{0, 1\}^n$, the resulting post-measurement state on subsystem BD is $((U_B P) \otimes \mathbb{I})|\psi\rangle_{BD}$, where $P = X^a Z^b$ is a Pauli gate.*

For a Clifford unitary V , an adaptive Pauli operation P' can correct the Pauli error P . This property arises from the ability to interchange a Pauli gate P with a Clifford unitary V . Specifically, $VP = V P V^\dagger = P' V$, where $P' = V P V^\dagger$ is also a Pauli gate due to the property of Clifford gates [70].

Lemma 2 (Clifford gate teleportation). *Let $|\mathbb{I}, V\rangle_{AB}$ and $|\psi\rangle_{CD}$ be two states, where A, B, C, D are n -qubit systems and V is an n -qubit Clifford gate. After performing Bell state measurements on subsystem AC and obtaining the measurement results \mathbf{a} and \mathbf{b} , where $\mathbf{a}, \mathbf{b} \in \{0, 1\}^n$, the resulting post-measurement state on subsystem BD are $(P' V \otimes \mathbb{I})|\psi\rangle_{BD}$, where $P = X^a Z^b$ and $P' = V P V^\dagger$ are Pauli gates.*

2. Spacetime conversion for random circuits

Here, we provide detailed proof of Theorem 2, which shows the spacetime conversion for random circuits. First, we introduce the concepts of projected ensembles and construct a random gate teleportation protocol. Then, we prove the spacetime conversion for random circuits using this protocol.

a. Projected ensemble

Let us define the projected ensemble of a state ensemble after measuring a subsystem.

Definition 2 (Projected ensemble of a state ensemble). *For a state ensemble $\mathcal{S} = \{p_i, |\psi_i\rangle_{AB}\}$ on systems A and B , the projected ensemble of \mathcal{S} on subsystem B after measuring subsystem A in the basis $\{|j_A\rangle\}$ is denoted as*

$$\{p_i q_{ij}, |\psi_{ij}\rangle\}, \quad (\text{A7})$$

where $q_{ij} = |(\langle j_A | \otimes \mathbb{I}_B) |\psi\rangle|^2$ represents the probability of obtaining measurement result j_A and $|\psi_{ij}\rangle = \frac{(\langle j_A | \otimes \mathbb{I}_B) |\psi\rangle}{\sqrt{q_{ij}}}$ represents the projected state on subsystem A .

Recall that $|U, V\rangle_{AB} = (U \otimes V) |\phi^n\rangle_{AB}$, where A and B are n -qubit quantum systems that are maximally entangled and U, V are n -qubit unitaries acting on A and B , respectively. We define the state ensembles by applying local random circuits on one side of the EPR pairs, i.e., the Choi states of local random circuits.

Definition 3 (Choi states of local random circuits). *Let A and B be two n -qubit systems. The state ensemble $\mathcal{E}_{n,t}$ is defined as the set of states generated by applying a local random circuit $U \in \mathcal{U}_{n,t}$ to the subsystem B of the EPR pairs $|\phi^n\rangle_{AB}$.*

$$\mathcal{E}_{n,t} = \{|I, U\rangle_{AB} : U_B \in \mathcal{U}_{n,t}\}. \quad (\text{A8})$$

This ensemble follows a probability distribution determined by $\mathcal{U}_{n,t}$.

The projected ensemble of $\mathcal{E}_{n,t}$ on subsystem B through computational-basis measurement on subsystem A yields the state ensemble $\mathcal{S}_{n,t}$, a consequence of the local unitary invariant property of Haar measure on $SU(4)$.

Lemma 3. *Consider the state ensembles $\mathcal{E}_{n,t}$ on systems A and B . The projected ensembles of $\mathcal{E}_{n,t}$ on system B through computational-basis measurement on subsystem A is the state ensemble $\mathcal{S}_{n,t}$.*

Proof. For any state $|\psi_{AB}\rangle = |I, U_B\rangle_{AB}$, the reduced density matrix on subsystem A is maximally mixed. Consequently, the measurement result j on subsystem A is uniformly distributed over $\{0, 1\}^n$, and the corresponding post-measurement state on subsystem B is $U_B |j\rangle_B$. Thus, the projected state ensemble is given by

$$\{U_B |j\rangle_B : U_B \in \mathcal{U}_{n,t}, j \in \{0, 1\}^n\}, \quad (\text{A9})$$

where the probability of U_B is determined by $\mathcal{U}_{n,t}$, and j is uniformly distributed over $\{0, 1\}^n$. This state ensemble is exactly $\mathcal{S}_{n,t}$ due to the local unitary invariant property of Haar random distribution on $SU(4)$. \square

b. Random gate teleportation

We show that two Choi states can be linked via Bell state measurements, resulting in Choi states of random circuits with increased circuit depth. This is achieved by teleporting the random circuits on one subsystem to another, a process we term random gate teleportation. This method is depicted in Fig. 7 and stated in the following lemma.

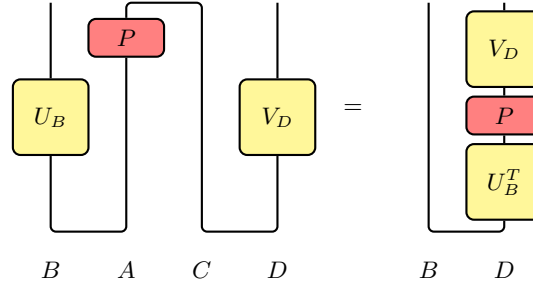


FIG. 7. Random gate teleportation. Systems A and B consist of n -qubit systems that are maximally entangled, with a local random circuit U_B of depth d_1 applied to system B . Systems C and D share a similar configuration, with a local random circuit V_D of depth d_2 on system D . The figure on the left-hand side shows the projected ensemble after performing Bell state measurements on subsystems AC , where P is the Pauli error distributed uniformly over $\{I, X, Y, Z\}^{\otimes n}$. The projected ensemble is equivalent to the right-hand side, which are Choi states of random circuits with increased circuit depth.

Lemma 4 (Random gate teleportation). *Given state ensembles \mathcal{E}_{n,d_1} on systems AB and \mathcal{E}_{n,d_2} on systems CD , where A, B, C , and D represent n -qubit quantum systems, through Bell state measurements on subsystems AC , the resulting projected ensemble on subsystems BD is $\mathcal{E}_{n,d'}$ with $d' = d_1 + d_2 - 1$ or $d' = d_1 + d_2$.*

Proof. Consider any states $|\psi\rangle_{AB} = |I, U_B\rangle_{AB}$ and $|\varphi\rangle_{CD} = |I, V_D\rangle_{CD}$. The reduced density matrix of the joint system $|\psi\rangle_{AB} \otimes |\varphi\rangle_{CD}$, restricted to subsystem AD , is maximally mixed. As a result, the outcomes \mathbf{a} and \mathbf{b} from the Bell state measurements on these subsystems are uniformly distributed over $\{0, 1\}^n$.

By applying Lemma 1, the post-measurement state can be expressed as:

$$\begin{aligned} |\psi_{\mathbf{ab}}\rangle_{BD} &= (U_B X^{\mathbf{a}} Z^{\mathbf{b}} \otimes I) |I, V_D\rangle_{BD} \\ &= |U_B X^{\mathbf{a}} Z^{\mathbf{b}}, V_D\rangle_{BD} \\ &= |I, V_D Z^{\mathbf{b}} X^{\mathbf{a}} U_B^T\rangle_{BD}, \end{aligned} \quad (\text{A10})$$

where the last equation is derived via Eq. (A5). Here, the unitaries U_B and V_D are sampled from \mathcal{U}_{n,d_1} and \mathcal{U}_{n,d_2} , respectively. The bit-strings \mathbf{a} and \mathbf{b} are uniformly distributed over $\{0,1\}^n$.

Due to the local unitary invariance and transpose-invariant properties of the Haar measure on $SU(4)$, $V_D Z^{\mathbf{b}} X^{\mathbf{a}}$ and U_B^T are still local random circuits with unchanged circuit depth. Consequently, the composition $(V_D Z^{\mathbf{b}} X^{\mathbf{a}} U_B^T)$ results in a local random circuit of depth d' , where $d' = d_1 + d_2$ if the first layer of V_D is staggered with the last layer of U_B^T , or $d' = d_1 + d_2 - 1$ if not. \square

c. Proof of Theorem 2

By integrating Lemma 3 with Lemma 4, we develop a method to construct state ensembles of local random circuits $\mathcal{S}_{n,t}$ using fewer layers of circuits via ancillary qubits and measurements. First, we show how to generate $\mathcal{E}_{n,t}$ with reduced depth.

Lemma 5. *Given a circuit depth t , there exists a circuit depth $t_1 \geq t$ such that for any even integer $k = 2m$, the state ensembles \mathcal{E}_{n,t_1} can be generated within a total depth of $d = \lfloor \frac{t}{k} \rfloor + 4$. This is achieved by employing a random circuit on kn qubits and performing Bell state measurements across $(k-2)n$ qubits.*

Proof. We partition $2mn$ qubits into m blocks, each containing $2n$ qubits. On each pair of qubits within the blocks, we prepare EPR pairs and apply local random circuits in \mathcal{U}_{n,d_2} on each side of EPR pairs separately, where $d_2 \geq \lfloor \frac{t}{2m} \rfloor + 2$. The state $|\phi^n\rangle$ within each block evolves to $|U_1, U_2\rangle = |I, U_2 U_1^T\rangle$, with U_1 and U_2 drawn from \mathcal{U}_{n,d_2} . This state represents a member of the ensemble \mathcal{E}_{n,d_3} , where $d_3 \geq 2d_2 - 1$.

By performing Bell state measurements to iteratively merge these blocks, we leverage Lemma 4 to obtain a final state from the ensemble \mathcal{E}_{n,t_1} in the last block, with $t_1 \geq d_3 m - m \geq t$. These Bell state measurements can be performed simultaneously in a single layer. Therefore, the total circuit depth is $d = 1 + d_2 + 1 = \lfloor \frac{t}{2m} \rfloor + 4$. \square

Then, we can prove Theorem 2 in the main text, which shows a spacetime conversion for random circuits.

Proof of Theorem 2. For the first claim, when $k = 2m$, we apply Lemma 5 to generate \mathcal{E}_{n,t_1} on kn qubits, where $t_1 \geq t$. Subsequently, a computational measurement is performed on one side of \mathcal{E}_{n,t_1} . According to Lemma 3, the projected ensemble is \mathcal{S}_{n,t_1} .

When $k = 2m + 1$, we set $d_2 = \lfloor \frac{t}{k} \rfloor + 2$. Following the protocol in Lemma 5, we generate \mathcal{E}_{n,d_3} with a depth of $d = d_2 + 2$ using $2mn$ qubits, where $d_3 \geq (2d_2 - 2)m$. Concurrently, we generate \mathcal{S}_{n,d_2+1} on the remaining n qubits. Bell state measurements are then performed on half of \mathcal{E}_{n,d_3} and \mathcal{S}_{n,d_2+1} . According to Lemma 4, the projected ensemble is \mathcal{S}_{n,t_1} , with $t_1 \geq d_2 + d_3 \geq t$. These Bell state measurements can be executed simultaneously with the previous measurements. The total depth is $\lfloor \frac{t}{k} \rfloor + 4$.

This procedure can be adapted to prove the second claim by applying a local random circuit of depth $d_2 + 1$ on the n -qubit state $|\phi\rangle$ instead of generating \mathcal{S}_{n,d_2+1} . The other steps is consistent with the proof of the first claim.

Finally, the circuit depth t_1 can be chosen equal to t by appropriately arranging the random circuits, which proves the theorem. \square

3. Spacetime conversion for Clifford circuits

Similar to Theorem 2, a spacetime conversion for implementing Clifford circuits can be established by utilizing the Clifford gate teleportation protocol in Lemma 2. First, we prove the following lemma.

Lemma 6. *Consider an n -qubit Clifford circuit $C = C_{2m} C_{2m-1} \cdots C_1$, where each component C_i is a Clifford circuit with a depth no greater than d . Using $(2m-2)n$ ancillary qubits, we can prepare the state $|\mathbb{I}, C\rangle_{AB}$ with a total circuit depth $d+2$, up to a Pauli error P on subsystem B . Consequently, the output state is $|\mathbb{I}, PC\rangle_{AB}$, and the Pauli error P is efficiently calculable.*

Proof. We divide the $2mn$ qubits into m blocks, each containing $2n$ qubits, and prepare EPR pairs within each block. For each i -th block, we apply the circuits $C_{2i-1}^T \otimes C_{2i}$ to the respective sides of the EPR pairs. According to Eq. (A5), the state $|\phi^n\rangle$ in the i -th block evolves to $|C_{2i-1}^T, C_{2i}\rangle = |\mathbb{I}, C_{2i} C_{2i-1}\rangle$.

We continue this process, merging the outputs of consecutive blocks using Bell state measurements as described in Lemma 2. Specifically, for the states $|\mathbb{I}, C_2 C_1\rangle$ and $|\mathbb{I}, C_4 C_3\rangle$, we apply the Bell state measurement to obtain $|\mathbb{I}, P_2 C_4 C_3 C_2 C_1\rangle$, where P_2 is a Pauli error. Repeating this for all blocks, we obtain:

$$|\mathbb{I}, P_m C_{2m} C_{2m-1} P_{m-1} C_{2m-2} C_{2m-3} \cdots C_1\rangle = |\mathbb{I}, P C_{2m} C_{2m-1} C_{2m-2} C_{2m-3} \cdots C_1\rangle = |\mathbb{I}, PC\rangle. \quad (\text{A11})$$

The Bell state measurements are performed simultaneously in a single layer, ensuring the overall circuit depth remains at $d + 2$, where the additional two layers account for the preparation of EPR pairs and the Bell state measurement. The Pauli error P can be efficiently calculated in the Heisenberg picture, as described in [70]. \square

Now, we can prove Theorem 4, which shows a spacetime conversion for implementing Clifford circuits.

Theorem 4 (Spacetime conversion for implementing Clifford circuits). *Given an n -qubit Clifford circuit that can be realized by single-qubit and two-qubit Clifford gate in depth t , for an integer $k \geq 2$, a reduced total depth $d = \lfloor \frac{t}{k} \rfloor + 4$ is sufficient to:*

1. Prepare the state $C|0\rangle^{\otimes n}$ by applying Clifford circuits of depth $d = \lfloor \frac{t}{k} \rfloor + 4$ on kn qubits and performing Bell state measurements along with computational measurements on $(k-1)n$ qubits and apply a Pauli gate on n qubits.
2. Apply the Clifford circuit C to any input state $|\phi\rangle$ when k is an odd number. This is achieved by applying a Clifford circuit on $|\phi\rangle$ and $(k-1)n$ ancillary qubits and performing Bell state measurements on $(k-1)n$ qubits and applying a Pauli gate on n qubits.

Proof. Given k , define $d_2 = \lfloor \frac{t}{k} \rfloor + 2$. Decompose C as $C = C_k C_{k-1} \dots C_1$, where each C_i represents a Clifford circuit of depth no greater than d_2 . For the first claim, when $k = 2m$, Lemma 6 enables the preparation of $|I, PC\rangle_{AB}$ within a depth of $d_2 + 2$. A computational basis measurement on subsystem A produces a result $\mathbf{a} \in \{0, 1\}^n$, leading to

$$|\varphi\rangle = PC|\mathbf{a}\rangle = PCX^{\mathbf{a}}|0\rangle^{\otimes n} = PP'C|0\rangle^{\otimes n}, \quad (\text{A12})$$

where $P' = CX^{\mathbf{a}}C^\dagger$ is a Pauli string. Then, the state $C|0\rangle^{\otimes n}$ can be obtained by applying $P'P$ to $|\varphi\rangle$.

When $k = 2m + 1$, denote $C' = C_{k-1}C_{k-2}\dots C_1$. One can prepare $|I, PC'\rangle$ and $C_k|0\rangle^{\otimes n}$ within a depth of $d_2 + 2$. Then, perform Bell state measurements on these two states and obtain measurement results \mathbf{a} and \mathbf{b} . The post-measurement state is

$$|\varphi\rangle = C_k P' P C' |0\rangle^{\otimes n} = P'' C |0\rangle^{\otimes n}, \quad (\text{A13})$$

where $P' = X^{\mathbf{a}}Z^{\mathbf{b}}$ and $P'' = C_k P' P C_k^\dagger$. Then, the state $C|0\rangle^{\otimes n}$ can be obtained by applying P'' to $|\varphi\rangle$. This method directly applies to the second claim by applying C_k to $|\phi\rangle$ instead of $|0\rangle^{\otimes n}$.

The last Bell state measurement and Pauli error correction are executed simultaneously with previous measurements in the final layer, ensuring the total circuit depth is $d = d_2 + 2 = \lfloor \frac{t}{k} \rfloor + 4$. \square

Appendix B: Bounding embedded complexity by circuit volume

We give here the proof of Theorem 1, which states that the embedded complexity of a projected state can be lower-bounded by circuit volume. The main technique in proving this theorem is to analyze the accessible dimension, which has been proven useful in understanding the complexity growth of random circuits [40, 41, 71], of post-measurement states. This dimension intuitively represents the degrees of freedom within a semi-algebraic set. Firstly, we establish a lower bound on the accessible dimension of post-measurement states. Then, we demonstrate how to bound embedded complexity by accessible dimension. Combining these findings, we establish the theorem.

To define the set of post-measurement states formally, consider the transformation from a local quantum circuit on an m -qubit system, constructed of d layers of two-qubit gates, to an n -qubit post-measurement state. This state results from measuring $m - n$ qubits and post-select the outcome 0^{m-n} . The total number of gates in the circuit is

$$V = \lfloor m/2 \rfloor d, \quad (\text{B1})$$

and the circuit consists of gates U_1, U_2, \dots, U_V . The mapping that takes V two-qubit gates as input and outputs the unnormalized post-measurement state can be written as:

$$G : SU(4)^V \rightarrow \mathbb{R}^M, \quad (\text{B2})$$

$$G(U_1, U_2, \dots, U_V) = (\langle 0|^{\otimes(m-n)} \otimes \mathbb{I}_{2^n}) U_V U_{V-1} \dots U_1 |0\rangle^m.$$

where $M = 2^{n+1}$ represents the degrees of freedom of unnormalized pure states. Denote the image of G by \mathcal{C} , which is the set of unnormalized post-measurement states. This set is a semi-algebraic set from the same argument as Observation 11 in [71].

Fact 1. *The set \mathcal{C} is a semi-algebraic set.*

Consequently, the set \mathcal{C} has a well-defined accessible dimension. By leveraging the random quantum teleportation technique in Theorem 2, we show that the accessible dimension of the set of post-measurement states is lower-bounded by circuit volume.

Lemma 7 (Lower bound on the accessible dimension). *The image \mathcal{C} of the mapping G has an accessible dimension D satisfying*

$$D \geq \min(L, 2^{n+1} - 1), \quad (\text{B3})$$

where $L = \frac{md}{2n^2} - m(1 + \frac{1}{n} + \frac{1}{n^2}) - 1$.

Proof. We consider the two-qubit gates acting on the first kn qubits, where $k = \lfloor \frac{m}{n} \rfloor \geq \frac{m}{2n}$, and set other gates to identity. In Theorem 2, we demonstrate that a total circuit depth of $\lfloor t/k \rfloor + 4$ is sufficient to generate the state ensemble $\mathcal{S}_{n,t}$ on these kn qubits. In that proof, the number of layers of random circuits after Bell state preparation is

$$d_1 = \lfloor t/k \rfloor + 2, \quad (\text{B4})$$

followed by Bell state measurement.

To perform Bell state preparation and measurement in a one-dimensional local circuit, one initially prepares EPR pairs between qubits 1 and $n+1$ using $n+1$ layers of gates. This involves swap operations to position qubits 1 and $n+1$ adjacently, executing a two-qubit gate, and restoring their original positions. By replicating this process for n additional times, Bell states are prepared between qubits i and $n+i$ for $1 \leq i \leq n$. Consequently, $n^2 + n$ layers are required to establish a maximally entangled state between qubits $1, 2, \dots, n$ and $n+1, n+2, \dots, 2n$. The preparation of the remaining EPR pairs can proceed in parallel. The same number of layers, $n^2 + n$, is adequate for Bell state measurement, leading to a total of $2(n^2 + n)$ layers for Bell state preparation and measurement.

After using $2(n^2 + n)$ layers for Bell state preparation and measurement, one utilizes $d_1 = d - 2(n^2 + n)$ layers for the random circuits in the middle section. The state ensemble $\mathcal{S}_{n,t}$ on the first n qubits is contained in the set of post-measurement states, where

$$t \geq k(d_1 - 2) \geq k[d - (2n^2 + 2n + 2)]. \quad (\text{B5})$$

It should be noted that the post-measurement state in the set \mathcal{C} remains unnormalized. Nevertheless, due to the properties of EPR pairs, the probability of obtaining $|0\rangle^{\otimes n}$ is consistently $c = 2^{-(k-1)n}$ (See Lemma 4). This leads to the relationship:

$$c\mathcal{S}_{n,t} \subseteq \mathcal{C}. \quad (\text{B6})$$

Additionally, $\mathcal{S}_{n,Ln} \subseteq \mathcal{S}_{n,t}$, where

$$\begin{aligned} L &= \lfloor t/n \rfloor \\ &\geq \left\lfloor \frac{k[d - (2n^2 + 2n + 2)]}{n} \right\rfloor \\ &\geq \frac{m[d - (2n^2 + 2n + 2)]}{2n^2} - 1 \\ &= \frac{md}{2n^2} - m(1 + \frac{1}{n} + \frac{1}{n^2}) - 1. \end{aligned} \quad (\text{B7})$$

In Appendix C of [40], it is shown that the accessible dimension of $\mathcal{S}_{n,Ln}$ has a lower bound:

$$\dim \mathcal{S}_{n,Ln} \geq \min(L, 2^{n+1} - 1). \quad (\text{B8})$$

Combining the above arguments, we have:

$$\dim \mathcal{C} \geq \dim \mathcal{S}_{n,t} \geq \dim \mathcal{S}_{n,Ln} \geq \min(L, 2^{n+1} - 1). \quad (\text{B9})$$

□

Moreover, we prove that the accessible dimension provides a lower bound for the embedded complexity.

Lemma 8 (Accessible dimension lower-bounds embedded complexity). *Suppose the image of the mapping G has an accessible dimension D . Consider randomly selecting V two-qubit gates U_1, U_2, \dots, U_V from $SU(4)^V$. With unit probability, the post-measurement state $|\phi\rangle = G(U_1, U_2, \dots, U_V)$ will satisfy $\|\phi\| \neq 0$, and the embedded complexity of the normalized state $|\psi\rangle = |\phi\rangle / \|\phi\|$ is lower-bounded by:*

$$C_{anc}(|\psi\rangle) \geq (D-1)/15. \quad (\text{B10})$$

Proof. Define $\mathcal{W}(s)$ as the space of unnormalized states generated by applying s two-qubit gates on $2s$ qubits, with measurements performed in the middle of the circuit, and in the final layer on the $2s-n$ ancillary qubits. We assume the measurement result is post-selected by $|0\rangle\langle 0|$. Any other measurement outcome would yield the same set $\mathcal{W}(s)$ due to the flexibility in choosing two-qubit gates. Here, we only consider the qubit number up to $2s$ because there are at most $2s$ qubits that are non-trivial support of the quantum gates.

Then, we define another set

$$\mathcal{V}(s) = \{c|\psi\rangle : c \in \mathbb{R}, c \geq 0, |\psi\rangle \otimes |0\rangle^{2s-n} \in \mathcal{W}(s)\}. \quad (\text{B11})$$

That is, we multiply the post-measurement state by a non-negative normalization number. By analyzing the free parameters, we have:

$$\dim \mathcal{V}(s) \leq 15s + 1. \quad (\text{B12})$$

Choose s_0 to be the largest integer such that $15s_0 + 1 < D$, then we have

$$\dim \mathcal{C} > \dim \mathcal{V}(s_0). \quad (\text{B13})$$

Following the same reasoning in [41], we decompose \mathcal{C} into $R \cup R^c$, where R is the set of regular points at which G has a maximal rank, and the complement R^c is the set of critical points. The preimage $G^{-1}(\mathcal{V}(s_0))$ of $\mathcal{V}(s_0)$ can then be expressed as:

$$(G^{-1}(\mathcal{V}(s_0)) \cap R^c) \cup (G^{-1}(\mathcal{V}(s_0)) \cap R). \quad (\text{B14})$$

The first term has measure zero because R^c has measure 0 as a subvariety since the rank can be characterized by minor determinants, which are polynomial functions. The second term also has measure zero because locally $(G^{-1}(\mathcal{V}(s_0)))$ are unions of submanifolds of R . Thus, the preimage of $\mathcal{V}(s_0)$ has measure zero in $SU(4)^V$.

Consequently, randomly draw V two-qubit unitaries U_1, U_2, \dots, U_V , with unit probability, the corresponding state $|\phi\rangle = G(U_1, U_2, \dots)$ will not be in the set $\mathcal{V}(s)$, thus the normalized state $|\psi\rangle = |\phi\rangle / \|\phi\|$ has an embedded complexity

$$C_{anc}(|\psi\rangle) \geq s_0 + 1 \geq (D-1)/15. \quad (\text{B15})$$

□

Combining Lemma 7 and Lemma 8, we establish a lower bound of embedded complexity by circuit volume.

Proof of Theorem 1. Lemma 7 shows that the accessible dimension of the image of G satisfies

$$D \geq \min(L, 2^{n+1} - 1), \quad (\text{B16})$$

where $L = \frac{md}{2n^2} - m(1 + \frac{1}{n} + \frac{1}{n^2}) - 1$. Consider randomly drawing two-qubit gates U_1, U_2, \dots, U_V , denote the state $|\phi\rangle = U_V U_{V-1} \dots U_1 |0\rangle^{\otimes m}$. From Lemma 8, we conclude that with unit probability, the probability of getting measurement result 0^{m-n} is non-zero, and the embedded complexity of the projected state $|\psi\rangle$ satisfies:

$$C_{anc}(|\psi\rangle) \geq (D-1)/15 = \min(L-1, 2^{n+1} - 2)/15. \quad (\text{B17})$$

This conclusion applies to an arbitrary measurement result, as applying random gates renders these measurement outcomes equivalent. Furthermore, since there are only a finite number of possible measurement results, with unit probability, all projected states have an embedded complexity satisfying Eq. (B17).

For $m \geq n \geq 4$, we have $L-1 \geq \frac{md}{2n^2} - 2m$. If $d \geq 5n^2$, we have $L-1 \geq \frac{md}{10n^2} = \Omega(\frac{V}{n^2})$. □

Appendix C: Approximate state design and approximate state complexity

In this section, we show that the random gate teleportation protocol links the circuit volume to approximate state design and approximate state complexity. First, we revisit their basic concepts and connections with local random circuits. Then, we discuss their connections with circuit volume.

1. Connection with local random circuits

a. Approximate state design

The randomness in a state ensemble $\mathcal{S} = \{p_i, |\psi_i\rangle\}$ can be quantified by a concept known as quantum state designs. A state ensemble \mathcal{S} is considered a quantum state t -design if it reproduces the first t moments of the Haar measure [57]. Concretely, the t th moments of state ensemble \mathcal{S} is calculated as

$$M_{\mathcal{S}}^{(t)} = \sum_i p_i |\psi_i\rangle\langle\psi_i|^{\otimes t}. \quad (\text{C1})$$

The Haar t th moments $M_{\text{Haar}}^{(t)}$ are defined on the Haar random ensemble, which is the uniform distribution over pure states in a Hilbert space. An ensemble \mathcal{S} is a state t -design if:

$$M_{\mathcal{S}}^{(t)} = M_{\text{Haar}}^{(t)}, \quad (\text{C2})$$

and it is an ϵ -approximate t -design if:

$$\left\| M_{\mathcal{S}}^{(t)} - M_{\text{Haar}}^{(t)} \right\|_1 \leq \epsilon, \quad (\text{C3})$$

where $\|\cdot\|_1$ denotes the trace norm. The approximate unitary t -design can also be defined similarly [72].

While Haar random states take an exponentially long time to prepare, quantum state designs can be generated using polynomially many gates. For example, random Clifford states are known to form state 3-designs [59]. Prior research indicates that local random circuits on n qubits can form ϵ -approximate t -designs in depth $d = \text{poly}(n, t, \epsilon)$ [72, 73], and the dependence on t was recently improved to linear scaling [42].

Fact 2 (Local random circuits are linear unitary t -design [42, Corollary 1.7]). *For $n \geq 2$ and $t \leq \Theta(2^{2n/5})$, the local random circuits on n qubits can form ϵ -approximate unitary t -design in depth $d = g(n, t, \epsilon)$, where*

$$g(n, t, \epsilon) = O\left(\left(nt + \log \frac{1}{\epsilon}\right)(\log t)^7\right). \quad (\text{C4})$$

Under the condition that $t \leq \Theta(2^{2n/5})$, $g(n, t, \epsilon)$ can be made $O(n^8 t)$, in which the dependence on ϵ are hidden.

b. Approximate state complexity

The approximate state complexity is a more robust version of the state complexity in a closed system, allowing a small trace distance δ to prepare the state.

Definition 4 (Approximate state complexity [72, Definition 3]). *The approximate δ -state complexity $C_{\delta}(\psi)$ of a pure state $|\psi\rangle$ is defined as the minimal number of two-qubit gates required to approximate the state to a trace distance δ :*

$$C_{\delta}(\psi) = \min\{V : U = U_V U_{V-1} \cdots U_1, \frac{1}{2} \left\| |\psi\rangle\langle\psi| - U(|0\rangle\langle 0|)^{\otimes n} U^\dagger \right\|_1 \leq \delta\}. \quad (\text{C5})$$

The two-qubit gates U_i can be arbitrary unitaries in $SU(4)$ and may act on any pair of qubits.

Recent results show a linear relation between approximate state design and approximate state complexity.

Fact 3 (Informal, [72, Theorem 3] [3]). *Let \mathcal{U} be a ϵ -approximate unitary t -design for some $t \leq O(2^{n/2})$. Then, $C_{\delta}(U|0\rangle^{\otimes n}) \geq \Omega(nt)$ with high probability.*

Here, the Ω notation hides the dependence on δ and ϵ . By combining Fact 2 and Fact 3, the growth of approximate state complexity for random state ensemble $\mathcal{S}_{n,t}$ can be established.

Lemma 9 (Approximate state complexity of random states). *Given $\delta \in (0, 1)$, $t \leq \Theta(2^{2n/5})$, randomly drawing a state $|\psi\rangle \in \mathcal{S}_{n,t}$, with high probability,*

$$C_{\delta}(|\psi\rangle) \geq \Omega\left(\frac{t}{n^7}\right). \quad (\text{C6})$$

Proof. By Fact 2, the state ensemble $\mathcal{S}_{n,t}$ forms an approximate k -design, where $k = \Omega\left(\frac{t}{n^8}\right)$. Then, by Fact 3, the state $|\psi\rangle \in \mathcal{S}_{n,t}$ has an approximate complexity

$$C_{\delta}(|\psi\rangle) = \Omega(nk) = \Omega\left(\frac{t}{n^7}\right). \quad (\text{C7})$$

with high probability. \square

2. Connection with circuit volume

The spacetime conversion for random circuits has significant implications for quantum state design and state complexity. Recently, considerable effort has been directed towards reducing the quantum circuit depth for generating quantum t -designs [42, 58, 60–62]. Our approach offers a simple yet powerful method to reduce the circuit depth by utilizing ancillary qubits. By combining Theorem 2 with Fact 2, we have:

Theorem 5 (State design via random gate teleportation). *For $n > O(\log t)$, an ϵ -approximate t -design on n qubits can be generated with total qubit number kn and circuit depth d , provided that $d \geq g(n, t, \epsilon)/k$.*

By inserting the expression of $g(n, t, \epsilon)$ in Fact 2, the order t of state design scales as

$$t = \Omega\left(\frac{kd}{n^8}\right) = \Omega\left(\frac{V}{n^9}\right), \quad (\text{C8})$$

where $V = \Theta(knd)$ represents the circuit volume. Our result shows that, with the utilization of ancillary qubits and measurements, the order t can scale linearly with the circuit volume V . This finding provides another operational meaning of circuit volume.

Additionally, the approximate complexity of the states generated by the random gate teleportation protocol can also be bounded by circuit volume.

Theorem 6 (Bounding approximate complexity by circuit volume). *Consider the n -qubit state ensemble $\mathcal{S}_{n,t}$ generated by Theorem 2, where the total qubit number is kn and the depth is $d = \lfloor \frac{t}{k} \rfloor + 4$. Randomly drawing a state $|\psi\rangle \in \mathcal{S}_{n,t}$, with high probability, the approximate complexity $C_\delta(|\psi\rangle)$ satisfies*

$$C_\delta(|\psi\rangle) \geq \Omega\left(\frac{V}{n^8}\right), \quad (\text{C9})$$

provided that $\delta \in (0, 1)$ and $d \leq \Theta(2^{2n/5})$. Here, $V = \Theta(knd)$ represents the circuit volume.

Proof. Theorem 2 shows that random circuits with depth d on kn qubits is enough to generate $\mathcal{S}_{n,t}$ on n qubits, where $t \geq k(d-4)$. By Lemma 9, these states has an approximate state complexity

$$C_\delta(|\psi\rangle) = \Omega\left(\frac{t}{n^7}\right) = \Omega\left(\frac{k(d-4)}{n^7}\right) = \Omega\left(\frac{V}{n^8}\right) \quad (\text{C10})$$

with high probability. □

These findings, derived from a specific construction, underscore how the design order and the approximate complexity of projected states in a subsystem scale with circuit volume. These findings further clarify the trade-off between space complexity and state complexity and provide evidence for the general behavior of approximate complexity growth of projected states.

Appendix D: Additional analysis for the ancilla-assisted shadow tomography

In this section, we delve deeper into the analysis of the ancilla-assisted shadow tomography. Initially, we examine the POVM operators associated with a chosen state ensemble and analyze their tomographical completeness. Subsequently, we detail the data processing schemes employed in our protocol. We demonstrate that our approach achieves performance comparable to the classical shadow protocol [45], particularly when the state ensemble is selected as state 3-designs or product random states.

1. POVM of a state ensemble

First, we analyze the POVM operators in the ancilla-assisted shadow tomography protocol. For a state ensemble \mathcal{S} and a given input state ρ in system $B = B_1 B_2 \cdots B_n$, we select a state $|\phi\rangle \in \mathcal{S}$ in system $A = A_1 A_2 \cdots A_n$ and perform a Bell state measurement on each pair of qubits $A_i B_i$. Let a_i and b_i denote the measurement results on the i -th qubit. Denote the unnormalized maximally entangled state as $|\Phi\rangle$, according to Eq. (A2) and Eq. (A6), the probability of obtaining bitstrings $\mathbf{a} = a_1 a_2 \cdots a_n$ and $\mathbf{b} = b_1 b_2 \cdots b_n$ is:

$$\begin{aligned}
p_{\mathbf{ab}}^\phi &= \frac{1}{2^n} \text{tr}\{[X_A^{\mathbf{a}}Z_A^{\mathbf{b}}(|\Phi\rangle\langle\Phi|)^{\otimes n}Z_A^{\mathbf{b}}X_A^{\mathbf{a}}]|\phi\rangle\langle\phi|\otimes\rho\} \\
&= \frac{1}{2^n} \langle\phi^*|X^{\mathbf{a}}Z^{\mathbf{b}}\rho Z^{\mathbf{b}}X^{\mathbf{a}}|\phi^*\rangle,
\end{aligned} \tag{D1}$$

where $|\phi^*\rangle$ denotes the complex conjugate of $|\phi\rangle$. Multiplying by the probability p_ϕ of chosen state ϕ in \mathcal{S} , this measurement result corresponds to a POVM operator

$$M_{\phi,P} = \frac{p_\phi}{2^n} P |\phi^*\rangle\langle\phi^*| P^\dagger, \tag{D2}$$

where $P = X^{\mathbf{a}}Z^{\mathbf{b}}$, $\mathbf{a}, \mathbf{b} \in \{0, 1\}^n$. Thus, for a given ensemble \mathcal{S} , the corresponding POVM operators are $\{M_{\phi,P}\}$.

2. Tomographical completeness

As long as these POVM operators are *tomographically complete*, it is possible to reconstruct the state and thus predict arbitrary properties of the state from the measurement results. Tomographic completeness is guaranteed if and only if for any two arbitrary states ρ and σ , there exists a Pauli string $P = X^{\mathbf{a}}Z^{\mathbf{b}}$ and a state $|\phi\rangle \in \mathcal{S}$ such that:

$$\begin{aligned}
\langle\phi^*|P^\dagger\rho P|\phi^*\rangle &\neq \langle\phi^*|P^\dagger\sigma P|\phi^*\rangle \\
\Rightarrow \langle\phi|P^\dagger(\delta\rho)^*P|\phi\rangle &\neq 0,
\end{aligned} \tag{D3}$$

where $\delta\rho = \rho - \sigma$. Notice that $\delta\rho$ can be an arbitrary traceless Hermitian matrix in \mathbb{H}_{2^n} up to a multiplicative factor. This characteristic gives the condition for the tomographical completeness of a state ensemble \mathcal{S} :

Theorem 7. *For a state ensemble \mathcal{S} , the corresponding POVM operators are tomographically complete if and only if the state ensemble \mathcal{S}' spans the space \mathbb{H}_{2^n} of traceless Hermitian matrices, where*

$$\mathcal{S}' = \{|\psi\rangle\langle\psi| : |\psi\rangle = P|\phi\rangle, |\phi\rangle \in \mathcal{S}, P = X^{\mathbf{a}}Z^{\mathbf{b}}, \mathbf{a}, \mathbf{b} \in \{0, 1\}^n\}. \tag{D4}$$

After choosing a tomographical-complete state ensemble, we can recover the state ρ from the measurement result [32, 45]. Concretely, the POVM maps the state ρ to the distribution of measurement outcomes P via a linear transformation M :

$$|\rho\rangle = \begin{pmatrix} \rho_{1,1} \\ \rho_{1,2} \\ \vdots \\ \rho_{d,d} \end{pmatrix} \xrightarrow{M} |P\rangle = \begin{pmatrix} P_1 \\ P_2 \\ \vdots \end{pmatrix}. \tag{D5}$$

Due to tomographic completeness, the linear transformation M has a left inverse R . For example, one can choose the Moore-Penrose pseudo-inverse:

$$R_{\text{MP}} = (M^\dagger M)^{-1} M^\dagger. \tag{D6}$$

To recover all the information in ρ , one can perform enough measurements to estimate $|P\rangle$ and apply the recovering map R :

$$|\rho\rangle = R|P\rangle. \tag{D7}$$

Although reconstructing the state might be expensive in sample complexity, our primary motivation is to measure properties instead of obtaining all the information about the state. In this case, one can predict some properties of ρ without fully recovering the state. Suppose we already perform M experiment and got measurement result $(|P_1\rangle, |P_2\rangle, \dots, |P_M\rangle)$, where $|P_i\rangle$ has a single '1' entry corresponding to the measurement result. The empirical unbiased estimator of $|P\rangle$ is

$$|\hat{P}\rangle = \frac{1}{M} \sum_{i=1}^M |P_i\rangle. \tag{D8}$$

To predict a given observable O , we write it in the vector form $|o\rangle$ and calculate the unbiased estimator of O as

$$(o|R|\hat{P}\rangle. \tag{D9}$$

The left inverse R is not unique, and the Moore-Penrose pseudo-inverse might not be optimal in sample complexity [32]. Moreover, the computational complexity for calculating the inverse is exponential in qubit numbers. In practice, we may devise clever methods to reduce the sample and computational complexity for specific state ensemble \mathcal{S} , as demonstrated next.

3. Case study: state 3-design and product random states

Here, we focus on two state ensembles: global random states and product random states. First, we introduce the classical data processing scheme when \mathcal{S} is a state 3-design and show that our protocol has equivalent performance to the classical shadow [45] using global random unitaries.

Suppose the Bell state measurement is performed on $|\phi\rangle \otimes \rho$, where $|\phi\rangle$ is drawn from a state 3-design \mathcal{S} , yielding measurement results $a_i, b_i \in \{0, 1\}$ for each qubit i . Let $\mathbf{a} = a_1 a_2 \cdots a_n$, $\mathbf{b} = b_1 b_2 \cdots b_n$ and $|b\rangle = Z^{\mathbf{b}} X^{\mathbf{a}} |\phi^*\rangle$. The protocol records the classical data as

$$\hat{\sigma} = (2^n + 1) |b\rangle\langle b| - \mathbb{I}_{2^n}. \quad (\text{D10})$$

This process is repeated N times, resulting in classical data $\{\hat{\sigma}_1, \hat{\sigma}_2, \dots, \hat{\sigma}_N\}$. As shown in Appendix D4, $\hat{\sigma}_i$ s are unbiased estimators of ρ . Thus, unbiased estimators of $\text{tr}(O\rho)$ can be obtained. To estimate the expectation value within the desired precision, the median-of-means technique proposed in [45] is applied. First, new classical data $\hat{\sigma}_{(k)}$ is calculated as follows:

$$\hat{\sigma}_{(k)} = \frac{1}{\lfloor N/K \rfloor} \sum_{l=(k-1)\lfloor N/K \rfloor + 1}^{k\lfloor N/K \rfloor} \hat{\sigma}_l. \quad (\text{D11})$$

For a given observable O , the prediction of $\text{tr}(\rho O)$ is then made by

$$\hat{\sigma} = \text{median}\{\text{tr}(O\hat{\sigma}_{(1)}), \text{tr}(O\hat{\sigma}_{(2)}), \dots, \text{tr}(O\hat{\sigma}_{(K)})\}. \quad (\text{D12})$$

The ancilla-assisted shadow tomography protocol based on state 3-design \mathcal{S} is summarized in Box 2.

Box 2: Ancilla-assisted shadow tomography based on state 3-design

Input:

1. N copies of an n -qubit state ρ .
2. Classical description of M observables O_1, O_2, \dots, O_M .

Protocol:

1. For each copy of ρ , randomly draw a state $|\phi\rangle \in \mathcal{S}$, where \mathcal{S} should be quantum state 3-design.
2. Perform Bell state measurement on each pair of qubits of $|\phi\rangle \otimes \rho$, yielding measurement results $a_i, b_i \in \{0, 1\}$ for $1 \leq i \leq n$. Let $\mathbf{a} = a_1 a_2 \cdots a_n$, $\mathbf{b} = b_1 b_2 \cdots b_n$, and $|b\rangle = Z^{\mathbf{b}} X^{\mathbf{a}} |\phi^*\rangle$. Record the classical data

$$\hat{\sigma} = (2^n + 1) |b\rangle\langle b| - \mathbb{I}. \quad (\text{D13})$$

3. Obtain N data points $\{\hat{\sigma}_1, \hat{\sigma}_2, \dots, \hat{\sigma}_N\}$ by repeating Steps 1 to Step 2 on N copies of ρ .
4. Split the data into K equally-sized parts, and set

$$\hat{\sigma}_{(k)} = \frac{1}{\lfloor N/K \rfloor} \sum_{l=(k-1)\lfloor N/K \rfloor + 1}^{k\lfloor N/K \rfloor} \hat{\sigma}_l. \quad (\text{D14})$$

5. Output the estimation of $\text{tr}(O_i \rho)$ as:

$$\hat{\sigma}_i = \text{median}\{\text{tr}(O_i \hat{\sigma}_{(1)}), \text{tr}(O_i \hat{\sigma}_{(2)}), \dots, \text{tr}(O_i \hat{\sigma}_{(K)})\}. \quad (\text{D15})$$

As proved in Appendix D4, this scheme exhibits equivalent performance to the original random Clifford measurement.

Proposition 1. *Ancilla-assisted shadow tomography protocol based on state 3-design depicted in Box 2 can predict the expectation value of M observables $\text{tr}(O_1 \rho), \text{tr}(O_2 \rho), \dots, \text{tr}(O_M \rho)$ to additive error ϵ , provided that $N \geq O(\frac{\log M}{\epsilon^2} \max_i \text{tr}(O_i^2))$.*

We can also choose \mathcal{S} as the tensor product of local random states. This state ensemble is well-suited for predicting local observables.

Proposition 2. *Ancilla-assisted shadow tomography using random states $|\phi\rangle = |\phi_1\rangle \otimes |\phi_2\rangle \otimes \dots \otimes |\phi_n\rangle$, where each $|\phi_i\rangle$ is uniformly drawn from $\{|0\rangle, |+\rangle = \frac{1}{\sqrt{2}}(|0\rangle + |1\rangle), |i+\rangle = \frac{1}{\sqrt{2}}(|0\rangle + i|1\rangle)\}$, can predict the expectation value of M arbitrary k -local observables $\text{tr}(O_1\rho), \text{tr}(O_2\rho), \dots, \text{tr}(O_M\rho)$ that satisfies $\max_i \|O_i\|_\infty \leq 1$ to additive error ϵ , provided that $N \geq O(\frac{\log M}{\epsilon^2} 4^k)$.*

To prove this proposition, note that the protocol is equivalent to measuring each qubit of the state ρ with six states:

$$\text{stab}_1 = \{|0\rangle\langle 0|, |1\rangle\langle 1|, |\pm\rangle\langle \pm|, |\pm i\rangle\langle \pm i|\}. \quad (\text{D16})$$

This is exactly the classical shadow protocol based on local random unitaries. Thus, this result can be derived by Proposition S3 in [45] and follows the same data postprocessing scheme. Suppose the measurement result on i -th qubit is $|\psi_i\rangle \in \text{stab}_1$, then, the classical data is recorded as:

$$\hat{\sigma} = \bigotimes_{i=1}^n \hat{\psi}_i, \quad \hat{\psi}_i = 3|\psi_i\rangle\langle\psi_i| - \mathbb{I}. \quad (\text{D17})$$

The rest of classical postprocessing is the same as in Box 2. This method is computationally efficient when the observables are local. Theorem 3 can be proved by combining Proposition 1 and Proposition 2.

Moreover, the method in [45] can be adopted to predict nonlinear functions $f(\rho)$. Given independent and unbiased estimators $\{\hat{\sigma}_1, \hat{\sigma}_2, \dots, \hat{\sigma}_N\}$, an unbiased estimators $\rho \otimes \rho$ of can be constructed as follows:

$$\hat{\mu}_2 = \frac{1}{N(N-1)} \sum_{i \neq j} \hat{\sigma}_i \otimes \hat{\sigma}_j. \quad (\text{D18})$$

A nonlinear function $\text{tr}(O\rho \otimes \rho)$ can be predicted by calculating $\text{tr}(O\hat{\mu}_2)$. This process can be repeated multiple times, and taking the median of these repetitions can reduce the prediction error. This allows for estimating nonlinear properties like the second Rényi entropy. Although the sample complexity remains exponential, there is a considerable reduction compared to brute-force methods such as full-state tomography. Additionally, this process can be generalized to higher moments of ρ by constructing unbiased estimators of $\rho^{\otimes k}$ via the U statistics [32, 45, 54]:

$$\hat{\mu}_k = \binom{N}{k}^{-1} \sum_{1 \leq i_1, \dots, i_k \leq N} \hat{\sigma}_{i_1} \otimes \hat{\sigma}_{i_2} \otimes \dots \otimes \hat{\sigma}_{i_k}. \quad (\text{D19})$$

4. Performance analysis of state 3-design

Here, we analyze the ancilla-assisted shadow tomography protocol based on state 3-design. Our analysis mainly follows the approach outlined in [45]. Suppose we perform Bell state measurement and get measurement result \mathbf{a}, \mathbf{b} . Let $|\phi, \mathbf{ab}\rangle = Z^{\mathbf{b}} X^{\mathbf{a}} |\phi^*\rangle$. According to Eq. (D1), the expectation value of $|\phi, \mathbf{ab}\rangle\langle\phi, \mathbf{ab}|$ is given by

$$\begin{aligned} \mathbb{E}_{\phi, \mathbf{ab}} |\phi, \mathbf{ab}\rangle\langle\phi, \mathbf{ab}| &= \mathbb{E}_{\phi} \sum_{\mathbf{ab}} p_{\mathbf{ab}}^{\phi} |\phi, \mathbf{ab}\rangle\langle\phi, \mathbf{ab}| \\ &= \frac{1}{2^n} \mathbb{E}_{\phi} \sum_{\mathbf{ab}} \langle\phi^*| X^{\mathbf{a}} Z^{\mathbf{b}} \rho Z^{\mathbf{b}} X^{\mathbf{a}} |\phi^*\rangle Z^{\mathbf{b}} X^{\mathbf{a}} |\phi^*\rangle\langle\phi^*| X^{\mathbf{a}} Z^{\mathbf{b}} \\ &= \frac{1}{2^n} \sum_{\mathbf{ab}} \mathbb{E}_{\phi} \langle\phi^*| X^{\mathbf{a}} Z^{\mathbf{b}} \rho Z^{\mathbf{b}} X^{\mathbf{a}} |\phi^*\rangle Z^{\mathbf{b}} X^{\mathbf{a}} |\phi^*\rangle\langle\phi^*| X^{\mathbf{a}} Z^{\mathbf{b}} \\ &= \frac{1}{2^n} \sum_{\mathbf{ab}} \frac{1}{2^n} \mathcal{D}_{1/(2^{n+1})}(\rho) \\ &= \mathcal{D}_{1/(2^{n+1})}(\rho). \end{aligned} \quad (\text{D20})$$

where $\mathcal{D}_p(\rho) = p\rho + (1-p)\frac{\mathbb{I}}{2^n}$. In the second equation, we use the equality

$$p_{\mathbf{ab}}^{\phi} = \text{tr}(|X^{\mathbf{a}} Z^{\mathbf{b}}, \mathbb{I}\rangle\langle X^{\mathbf{a}} Z^{\mathbf{b}}, \mathbb{I}| [|\phi\rangle\langle\phi| \otimes \rho]) = \frac{1}{2^n} \langle\phi^*| X^{\mathbf{a}} Z^{\mathbf{b}} \rho Z^{\mathbf{b}} X^{\mathbf{a}} |\phi^*\rangle. \quad (\text{D21})$$

In the third equation, we swap the order of summation. The fourth equation leverages the 3-design property of \mathcal{S} . For the Hermitian matrix in \mathbb{H}_{2^n} and a Pauli string $P = Z^{\mathbf{b}}X^{\mathbf{a}}$, we have:

$$\mathbb{E}_{\phi} P |\phi^*\rangle\langle\phi^*| P^\dagger |\phi^*\rangle\langle\phi^*| A P |\phi^*\rangle = \frac{A + \text{tr}(A)\mathbb{I}}{(2^n + 1)2^n} = \frac{1}{2^n} \mathcal{D}_{1/(2^n+1)}(A) \text{ for } A \in \mathbb{H}_{2^n}, \quad (\text{D22})$$

$$\mathbb{E}_{\phi} P |\phi^*\rangle\langle\phi^*| P^\dagger |\phi^*\rangle\langle\phi^*| B_0 P |\phi^*\rangle\langle\phi^*| P^\dagger C_0 P |\phi^*\rangle = \frac{\text{tr}(B_0 C_0)\mathbb{I} + B_0 C_0 + C_0 B_0}{(2^n + 2)(2^n + 1)2^n} \text{ for } B_0, C_0 \in \mathbb{H}_{2^n} \text{ traceless.} \quad (\text{D23})$$

Now, we analyze the estimator $\hat{o} = \text{tr}(O\hat{\sigma})$. The expectation of the data $\hat{\sigma}$ satisfies

$$\begin{aligned} \mathbb{E}\hat{\sigma} &= \mathbb{E}_{\phi, \mathbf{ab}}[(2^n + 1) |\phi, \mathbf{ab}\rangle\langle\phi, \mathbf{ab}| - \mathbb{I}] \\ &= (2^n + 1)\mathbb{E}_{\phi, \mathbf{ab}}[|\phi, \mathbf{ab}\rangle\langle\phi, \mathbf{ab}|] - \mathbb{I} \\ &= (2^n + 1)\mathcal{D}_{1/(2^n+1)}(\rho) - \mathbb{I} \\ &= \rho. \end{aligned} \quad (\text{D24})$$

Thus,

$$\mathbb{E}\hat{o} = \mathbb{E}\text{tr}(O\hat{\sigma}) = \text{tr}(O\mathbb{E}\hat{\sigma}) = \text{tr}(O\rho). \quad (\text{D25})$$

That is, \hat{o} is an unbiased estimator of $\text{tr}(O\rho)$. Next, we analyze the variance of \hat{o} . Define the linear map $\mathcal{M} = \mathcal{D}_{1/(2^n+1)}$, according to Lemma S1 in [45], we have

$$\text{Var}[\hat{o}] = \mathbb{E}[(\hat{o} - \mathbb{E}[\hat{o}])^2] \leq \|O_0\|_{\text{shadow}}, \quad (\text{D26})$$

where $O_0 = O - \frac{\text{tr}(O)}{2^n}\mathbb{I}$, and the shadow norm is defined as

$$\|O\|_{\text{shadow}} = \max_{\sigma: \text{state}} (\mathbb{E}_{\phi} \sum_{\mathbf{ab}} p_{\mathbf{ab}}^{\phi} \langle\phi, \mathbf{ab}| \mathcal{M}^{-1}(O) |\phi, \mathbf{ab}\rangle)^2)^{1/2}. \quad (\text{D27})$$

Here, we establish the bound of shadow norm for the ancilla-assisted shadow tomography.

Proposition 3 (Shadow norm for ancilla-assisted shadow tomography). *For any observable O , its traceless part $O_0 = O - \frac{\text{tr}(O)}{2^n}\mathbb{I}$ satisfies*

$$\|O_0\|_{\text{shadow}}^2 \leq 3\text{tr}(O^2). \quad (\text{D28})$$

Proof. Following Eq. (S42) in [45], we have

$$\mathcal{M}^{-1}(O_0) = (2^n + 1)O_0 \quad (\text{D29})$$

for any traceless $O_0 \in \mathbb{H}_{2^n}$. Then, from Eq. (D20) and Eq. (D27), we have

$$\begin{aligned} \|O_0\|_{\text{shadow}}^2 &= \max_{\sigma: \text{state}} \left(\frac{1}{2^n} \mathbb{E}_{\phi} \sum_{\mathbf{ab}} \langle\phi^*| X^{\mathbf{a}} Z^{\mathbf{b}} \sigma Z^{\mathbf{b}} X^{\mathbf{a}} |\phi^*\rangle [\langle\phi^*| X^{\mathbf{a}} Z^{\mathbf{b}} (2^n + 1) O_0 Z^{\mathbf{b}} X^{\mathbf{a}} |\phi^*\rangle]^2 \right) \\ &= \max_{\sigma: \text{state}} \text{tr} \left(\sigma \frac{1}{2^n} \sum_{\mathbf{ab}} \mathbb{E}_{\phi} Z^{\mathbf{b}} X^{\mathbf{a}} |\phi^*\rangle\langle\phi^*| X^{\mathbf{a}} Z^{\mathbf{b}} [\langle\phi^*| X^{\mathbf{a}} Z^{\mathbf{b}} (2^n + 1) O_0 Z^{\mathbf{b}} X^{\mathbf{a}} |\phi^*\rangle]^2 \right) \\ &= \max_{\sigma: \text{state}} \text{tr} \left(\sigma 2^n \frac{(2^n + 1)^2 (\text{tr}(O_0^2)\mathbb{I} + 2O_0^2)}{(2^n + 2)(2^n + 1)2^n} \right) = \frac{2^n + 1}{2^n + 2} \max_{\sigma: \text{state}} (\text{tr}(\sigma)\text{tr}(O_0^2) + 2\text{tr}(\sigma O_0^2)). \end{aligned} \quad (\text{D30})$$

Note that $\text{tr}(\sigma O_0^2) \leq \|O_0\|_{\infty}^2 \leq \text{tr}(O_0^2)$, $\text{tr}(\sigma) = 1$ and $\text{tr}(O_0^2) = \text{tr}(O^2) - \frac{\text{tr}(O)^2}{2^n} \leq \text{tr}(O^2)$. Thus, we obtain Eq. (D28). \square

After obtaining the shadow norm of the operator, we bound the variance of \hat{o} according to Eq. (D26):

$$\text{Var}[\hat{o}] \leq 3\text{tr}(O^2). \quad (\text{D31})$$

Directly applying concentration inequalities to \hat{o} is not feasible because \hat{o} and its higher moments are not yet bounded. To address this, we employ the median-of-means method, following [45]. Firstly, we average B estimators

to obtain $\hat{\sigma}_{(l)} = \hat{\sigma}_{(l-1)B+1}, \hat{\sigma}_{(l-1)B+2}, \dots, \hat{\sigma}_{lB}$, where $\hat{\sigma}_i$ are independent and identically distributed estimators. The estimator $\hat{\sigma}_{(l)}$ remains unbiased, and its variance is suppressed by B through standard calculations, yielding:

$$\text{Var}[\hat{\sigma}_{(l)}] \leq \frac{3\text{tr}(O^2)}{B}. \quad (\text{D32})$$

Setting $B = \frac{30\text{tr}(O^2)}{\epsilon^2}$, we ensure $\text{Var}[\hat{\sigma}_{(l)}] \leq \frac{\epsilon^2}{10}$. By Markov's inequality, we have:

$$\Pr[|\hat{\sigma}_{(l)} - \text{tr}(O\rho)| > \epsilon] \leq \frac{\text{Var}[\hat{\sigma}_{(l)}]}{\epsilon^2} \leq \frac{1}{10}. \quad (\text{D33})$$

Now, we apply Hoeffding's inequality to the indicator function $\mathbb{1}_{|\hat{\sigma}_{(i)} - \text{tr}(O\rho)| > \epsilon}$. After calculating the median m of $\hat{\sigma}_{(1)}, \hat{\sigma}_{(2)}, \dots, \hat{\sigma}_{(K)}$, the probability that $|m - \text{tr}(O\rho)| > \epsilon$ is equal to the probability that

$$\frac{1}{K} \sum_{i=1}^K \mathbb{1}_{|\hat{\sigma}_{(i)} - \text{tr}(O\rho)| > \epsilon} \geq \frac{1}{2}. \quad (\text{D34})$$

According to Hoeffding's inequality, this probability will be $\exp(-O(K))$.

Given M observables, by setting $B = \frac{30 \max_i \text{tr}(O_i^2)}{\epsilon^2}$ and $K = O(\log \frac{M}{\delta})$, the probability that there exists an estimation m_i of $\text{tr}(O_i\rho)$ such that $|m_i - \text{tr}(O_i\rho)| > \epsilon$ is at most

$$M \exp(-O(K)) \leq \delta \quad (\text{D35})$$

by a union bound. Thus, to estimate any $\text{tr}(O_i\rho)$ up to an additive error of ϵ with probability δ , choosing $N = BK = O\left(\frac{\log \frac{M}{\delta}}{\epsilon^2} \max_i \text{tr}(O_i^2)\right)$ suffices.